MASTER THESIS

ESTIMATION OF JOINT STIFFNESS VIA A MUSCULOSKELETAL MODEL DRIVEN BY MOTOR NEURON TWITCH PROPERTIES

Sainivedhitha Arunajatesan

FACULTY OF ENGINEERING TECHNOLOGY
DEPARTMENT OF BIOMECHANICAL ENGINEERING

EXAMINATION COMMITTEE
prof. dr. ir. M. Sartori
dr. S. U. Yavuz
ir. C. P. Cop
ir. A.D.J. Gogeascoechea Hernandez

DOCUMENT NUMBER
BE - 917

Estimation of Joint Stiffness via a Musculoskeletal Model Driven by Motor Neuron Twitch Properties

SAINIVEDHITHA ARUNAJATESAN
University of Twente, Enschede, The Netherlands

***Abstract*—Joint stiffness estimation involves joint perturbation or torque-based experiments in conjunction with system identification techniques. The modeling techniques recently used to estimate joint stiffness include bipolar ElectroMyoGraphy (EMG) data to drive the musculoskeletal model. These models do not provide detailed information on individual Alpha Motor Neuron (α-MN) properties which is essential to improve the personalization of the Neuro Musculo Skeletal (NMS) model. The use of bipolar electrodes limits the resolution to extract the α-MN properties. In this study, the NMS models were driven by the activation dynamics of EMG envelopes and motor unit activation dynamics, respectively. The normalized EMG envelopes were regarded as the activation profiles of EMG envelopes. For the activation dynamics of motor units, the Motor Units (MUs) were decomposed from uni-polar HD-EMG data using a blind source separation technique, and the motor unit distributions were sampled to formulate the activation profiles. The experimental torque from the Achilles and stiffness estimation from System Identification (SI) technique were used as a reference to validate the results of the models at the torque and stiffness level. The torque estimations by both models were better than the stiffness estimations. At the torque level, the model driven by motor units produced improved results; at the stiffness level, the model driven by EMG envelopes produced better results. Overall, this method can be used to predict the torque but enhancements should be made to increase the stiffness estimation results. Further, the entire study was performed under isometric conditions. The inclusion of unique properties of isometric conditions such as Short Range Stiffness (SRS) in the future could improve the results.**

I. INTRODUCTION

Humans move as a result of muscles operating on skeletal joints to provide mechanical output from afferent and efferent brain activity. Such outputs are then translated into the exchange of interaction forces with the environment. Humans are adept at physically interacting with the surrounding across a wide range of topographies and automatically adapting to their demands. This effective adaptation process usually requires little to no conscious thought. It is primarily controlled at the neuromuscular level by constant viscoelastic characteristic modification in various Musculo Tendon Units (MTUs) [1]. The concept of MTU viscoelasticity at the joint level can be conveyed through the use of joint impedance. Joint impedance is a measure of the resistance to motion of a joint in the human body. Impedance has three components: inertial contributions, damping, and stiffness. Joint stiffness is responsible for storing and releasing energy based on the position [2]. The method to measure the joint stiffness, *invivo*, is difficult during movement.

The strategies that may be used to quantify the joint stiffness *invivo* are: *Ultrasound Elastography*, *System Identification*, and *Musculoskeletal modeling*.

Ultrasound Elastography uses ultrasound to measure the mechanical properties and stiffness of the tissue. This can be performed either by applying stress or shear waves to the tissues and measuring the tissue deformation. This technique provides a less-quantitative tissue stiffness measurement compared to other techniques, making it harder to use for joint stiffness estimation [3]. So, a quantitative measurement is required to estimate joint stiffness.

System identification is a quantitative and comprehensive assessment of joint stiffness estimation. It calculates the values of dynamic movement parameters such as mass, inertia, damping, stiffness, and time constants in a particular model structure using input and output signals measured from the system. The stiffness estimation during movement is a time-varying property and there are three kinds of time-varying system identification techniques used: ensemble, Short Data Segment (SDS), and Basis Impulse Response Function (BIRF) [4]. Even though BIRF and SDS were used in studies and produced fewer error rates, SDS has access to limited frequency and cannot capture complex joint dynamics and BIRF has limited applicability as it makes many assumptions that usually are not valid in experimental setups [5]. On the other hand ensemble-averaging techniques, which

estimate time-varying variables using a large set of input/output realizations with the same underlying time-varying patterns, are actively used to estimate joint stiffness [6], [5]. System identification typically relies on measuring the motion of a joint and the forces applied to it, without taking into account the underlying musculoskeletal anatomy and physiology which is one of the main disadvantages. As a result, it may not provide a complete picture of how joint stiffness is influenced by muscle activation and other factors. On the other hand, musculoskeletal modeling can provide a more detailed and comprehensive representation of the musculoskeletal system, including the underlying anatomy and physiology of the joints and muscles. This can lead to more accurate and realistic estimates of joint stiffness.

Muscles with origin and insertion locations on a skeleton typically made up of anatomically accurate bone geometry are represented in musculoskeletal models. To activate multiple MUs in a physiologically accurate model of the human musculoskeletal system, EMG recordings obtained from major muscle groups are utilized [7]. Joint stiffness during dynamic activity may be estimated using EMG-driven musculoskeletal modeling without the need to disturb the joint [1].

Through *EMG-driven musculoskeletal modeling*, Cop et al. created a unique "perturbation-free" stiffness estimation approach that was first tested against system identification methods [8], [9]. Model-based estimations of joint stiffness were comparable to methods of system identification. When a muscle is activated, motor units generate force, which causes a change in muscle length and stiffness. Therefore, a model that accurately represents the stiffness of a joint needs to consider the properties of the motor units responsible for generating the forces that affect joint stiffness. EMG-driven musculoskeletal models estimate overall muscle activation based on surface EMG signals [9]. The aforementioned model did not provide information on individual α-MN properties that can simulate the muscle activation in greater detail. By using only the EMG signals, the results are prone to more errors as the EMG signals might be affected by factors such as electrode placement and skin impedance. The addition of motor unit properties to a model eliminates this disadvantage. Further, the decomposition of motor units can extract the motor unit firing capacity at different frequencies [10], [11].

Each muscle is made up of several motor units that interact with one another to govern both the coarse and fine movements of the muscle. A lower motor neuron and the fibers of skeletal muscle it innervates make up a motor unit [12]. Muscle control may be significantly impacted by changes in motor unit structure or function brought on by aging or illness [13]. It has been shown that the ratio of rapid to slow motor units within a muscle affects the overall twitch properties of that muscle [14]. The fast and slow motor units are classified based on the recruitment threshold, the force level achieved at the instance at which the first firing of the motor unit occurs. The slow motor units recruit earlier, meaning that they have a lower threshold, and vice versa in fast motor units.

Our inadequate knowledge of the connection between the neural and mechanical levels of human movement currently impedes the development of neuroprostheses. Because human motor function varies greatly between individuals and motor activities, current neurorehabilitation systems work in an open-loop system and rely on evaluation. This prevents people who have suffered neurological damage from fully regaining their motor skills [15]. The non-invasive diagnosis and characterization of abnormal neurological patterns are made possible by access to motor neuron information [16].

This prompts further research into how spinal motor circuits react to mechanical or electrical inputs. Through signal-driven neuro-musculoskeletal models, Hernandez et al. [15] sought to connect such *invivo* methods with the mechanical output. They presented several methods for collecting motor units *invivo* and connecting them to the mechanisms that cause a force to be generated during human movement. Their approach produced reliable activation patterns that were very comparable to reference torques [15]. The ability to decompose several MUs from high density-EMG [17] opens new avenues to extend current generalized neuromusculoskeletal models into MU-specific formulations.

This research is necessary because the knowledge gap between the neural and muscular systems was bridged by the ability to estimate joint stiffness at any time without the need to perform joint perturbations [8]. However, the EMG-driven musculoskeletal models did not provide detailed information on individual α-MN properties [18]. The work on motor units for neuroprosthesis development led to further research of the effect on results when the musculoskeletal models are driven with MU-specific formulations.

The main aim of this research is to:

1) **Develop a comprehensive neuromusculoskeletal framework that combines stiffness estimation and the identification of motoneuron properties.**
2) **Compare the aforementioned model to the musculoskeletal framework driven by EMG envelopes to witness if the model has improved estimation of joint torque and stiffness.**
3) **Validate the predicted results with the experimental results and the system identification**

methods in a controlled dynamic ankle stiffness estimation experiment.

II. Methods

A. Data Collection

The study involved six individuals who were in good health. All experimental procedures were approved by the Ethical Committee of the University of Twente, and written informed consent was obtained from all participants. The dynamic trials to apply perturbation and measure the position and torque of the ankle joint were conducted using the Achilles Rehabilitation Device (MOOG, Nieuw-Vennep, The Netherlands), which is a single-axis manipulator controlled by admittance. Figure 1 depicts the device used in the study.

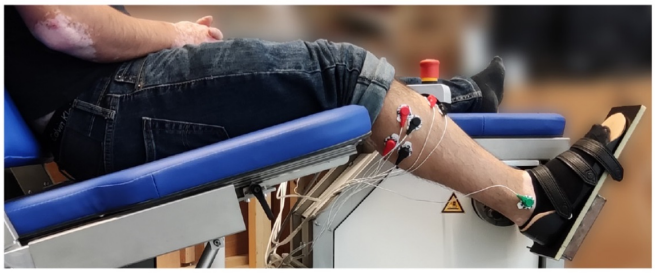

Fig. 1: Electrode and marker placement on the subject during the experiment in Achilles to determine ankle stiffness. Figure adapted from [9]

The experimental setup was consistent with that of a previous study [9]. Using the Achilles Rehabilitation Device, the participants performed torque tracking tasks and were instructed to complete a maximum voluntary contraction trial without any equipment assistance. To create a viscoelastic virtual environment that would resist movement, the Achilles device was configured to replicate virtual parameters of inertia, damping, and stiffness of 0.1 kg·m^2, 2.5 N·m·s·rad^{-1}, and 4500 N·m·rad^{-1}, respectively. The Refa system (TMSi, Oldenzaal, The Netherlands) was used to record EMG activity at a frequency of 2048 Hz. The muscles under interest were Tibialis Anterior (TA), Soleus (Sol), Gastrocnemius medialis (GM), Gastrocnemius lateralis (GL), and Peroneus longus (PL). The EMG data were collected using two 64-channel electrodes were used for TA and Sol, three bipolar electrodes were used for GM, GL, and PL, and a 132-channel amplifier. Channels 1-64 corresponded to TA, 65-128 to Soleus, 129 to GM, 130 to GL, and 131 to PL. The knee angle was manually measured and set to 30 degrees knee flexion via a hand-held goniometer at the beginning of the experiment, and subjects were instructed to not move the knee. The initial ankle angle was also measured and set to 10 degrees plantar flexion with the aid of the goniometer. The subjects were instructed to oscillate their ankle by tracking a 0.5 Hz target sine torque around the initial ankle angle. Each subject performed eight trials under the same experimental conditions. The EMG data were obtained under the condition (as shown in Figure 2): Static where only perturbation was applied (40-80 sec).

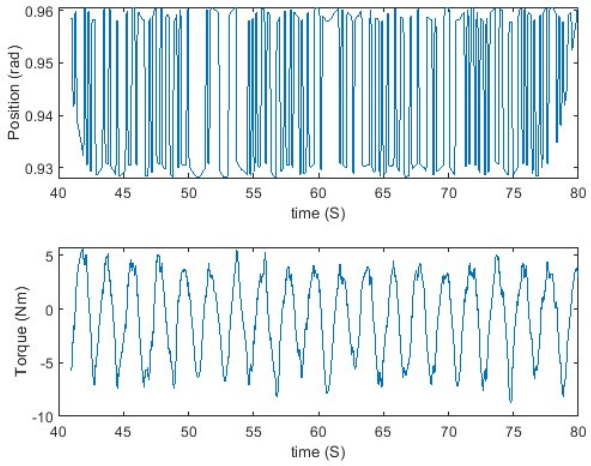

Fig. 2: Plot of position and torque data indicating the experimental condition

B. Data Processing

1) EMG data: Both the mono-polar and bi-polar HD-EMG data and torque data from Achilles were processed using MATLAB R2022a (The Mathworks Inc., Natick, MA, USA) [19]. The EMG data were synchronized by finding the delay between the raw EMG data and the synchronization signal. The synchronized EMGs were plotted against a time vector and showed drastic fluctuations in a few channels as shown in Figure 3a that might be due to electrode connection error. The channels with drastic change were removed based on the difference of amplitude between adjacent values (Figure 3b) and filtered using two different zero-phase second-order IIR notch filters - one that filters only 50Hz signal and another that filters harmonics up to 500Hz.

It was concluded to use a notch filter of only 50 Hz as this took less running time and both worked quite similarly in further decomposition. The 50Hz notch filtered signal was again filtered using a zero-phase fourth-order Butterworth band pass filter (20-500Hz), rectified, and the envelopes were found by utilizing a fourth-order Butterworth low-pass filter with zero-phase of cut-off frequency 5Hz. These processes were verified using a periodogram.

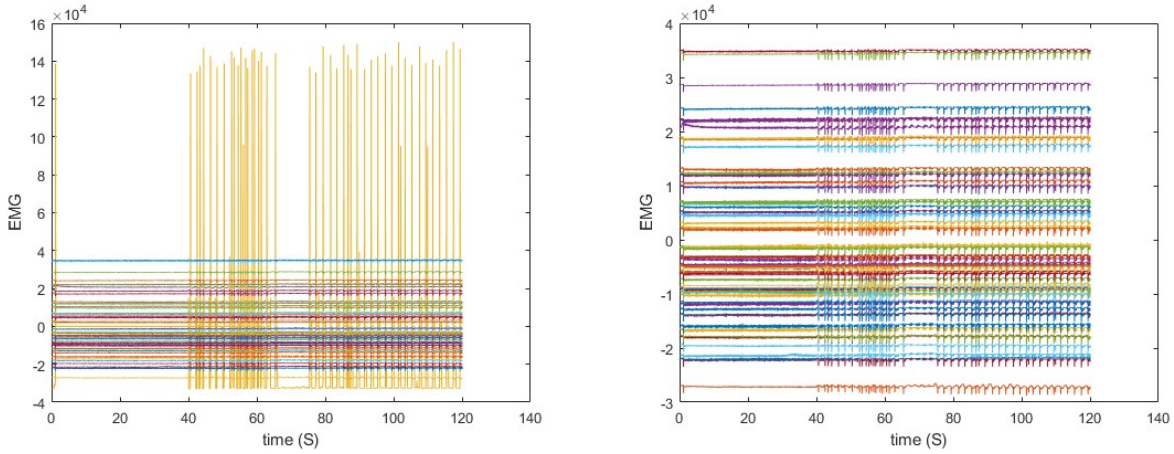

(a) Synchronized EMG vs time of all the channels (b) Synchronized EMG vs time after outlier removal

Fig. 3: Plot of synchronized EMG data against time vector

2) MVC data: In humans, maximal voluntary contraction (MVC) refers to the highest capacity of a muscle or a group of muscles to generate force. The MVC data of each subject were processed in the same way as the EMG data and the MVC envelopes were found.

3) Activation Dynamics of EMG Envelope: The mean of all the channels of the respective muscles of the EMG and MVC envelopes were calculated. The mean of EMG envelopes was normalized using the maximum value of the mean of the MVC envelope and stored as Activation Dynamics (AD) of EMG envelopes in the form of time series data for joint torque and stiffness estimation.

C. Decomposing Motor Units

The bandpass filtered EMG signals were then decomposed into constituent MU spike trains and Innervation Pulse Trains (IPTs) using a convolutive blind source separation technique called Convolution Kernel Compensation [20]. IPTs are the whole sequences of electrical pulses during voluntary muscle contractions. IPT refers to the pattern of electrical impulses that are sent from motor neurons to muscles during muscle contraction. The properties of motor units are determined by the number and properties of the muscle fibers they innervate.

For every MU spike train, a vector was generated, in which a value of 1 represented the firing (discharge) event of the respective motor unit. The value 0 was used in all time frames where no discharge was detected [15]. The quality of these motor units decomposed was assessed using the Pulse Noise Ratio (PNR) which directly relates to the quality of the decomposition (i.e., the ratio between pulse energy and noise level) [21]. The PNR was expressed in dB and defined as the logarithmic ratio between the average innervation pulse train at the estimated time moments when a MU discharged ($E(\hat{t}^2(n)|_{\hat{t}^2(n)=1})$ and when it did not discharge ($E(\hat{t}^2(n)|_{\hat{t}^2(n)=0})$ [21].

$$PNR(\hat{t}(n)) = 10 * log_{10}\frac{(E(\hat{t}^2(n)|_{\hat{t}^2(n)=1})}{(E(\hat{t}^2(n)|_{\hat{t}^2(n)=0})} \quad (1)$$

As per the works of Gogeascoechea et al., the PNR threshold was 20dB [22] and Holobar et al., revealed that the majority of MUs with PNR above 30dB [21]. The Pulse to Noise Ratios was plotted in the form of a histogram to determine the threshold. From Figure 4, the threshold of 20dB included most of the MU spike trains, and on visual inspection, they looked physiologically correct.

Motor units having PNR $<$ 20dB were discarded from the analysis. After quality selection, the mean discharge rates (DR) were calculated for each motor unit spike train. Discharge Rate is defined as the mean inverse difference of the time elapsed between consecutive spikes [15].

$$DR = \frac{1}{N-1}\sum_{i=2}^{N}\frac{1}{t_i - t_{i-1}} \quad (2)$$

The TA represents dorsiflexion while Sol, GM, GL, and PL represents plantar-flexion [23]. The data corresponding to the dorsiflexion should lie in the increasing torque data while the plantar flexion should lie in the decreasing torque data. This can be visualized when the respective data is plotted against torque data as shown in Figure 5. The MU spike trains of the Tibialis Anterior that lie in the dorsiflexion and of the Soleus lie in

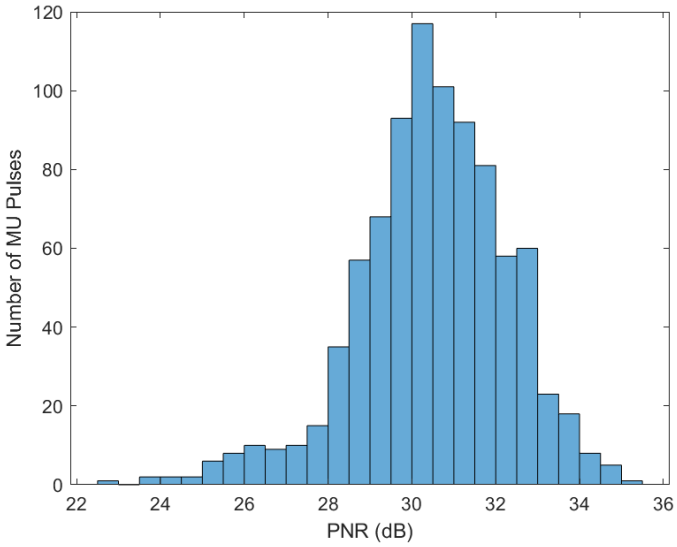

Fig. 4: Histogram of pool of PNR values of all trials and subjects

the plantar flexion were included in the further analysis while the other MU spike trains were removed. All motor units were manually analyzed and the motor unit spike trains with several spikes greater than 500 and less than 100 was found to be non-reliant. The 100 spikes in 40 seconds mean that the motor unit had many silent periods which was considered not useful for further analysis. The motor units with more than 500 spikes did not correspond to the respective flexion i.e., they had spikes in both the flexion making it difficult to analyze, and had PNR<20dB. So, these were removed and only motor units with a reliable discharge pattern were considered for the analysis.

Then the recruitment thresholds (RT) were calculated which is the value of the AD of EMG data where the first spikes of the MU spike trains strike. Usually, RT is found with the help of MVC force profiles. In this situation, the MVC data was measured using an Achilles device which has a disadvantage in that it cannot measure very high torque data. So, instead of the MVC force profiles, EMG Envelopes were used. The point of recruitment on the AD of the EMG envelope is shown in Figure 6.

Simply relying on these characteristics does not provide a definitive way to differentiate between different types of motor units. Without additional analysis, accurately predicting twitch properties becomes more difficult. To address this issue, a linear combination or eigenvector was identified that could maximize the variance of the decomposed motor unit features. To achieve this, the mean discharge rates were first normalized to a maximum value of 40 Hz as done by Gogeascoechea et al., [15]. As shown in Figure 7, the dimensionality was reduced by extracting the first principal component and projecting the data onto the first eigenvector.

TABLE I: CONTRACTION TIMES OF TIBIALIS ANTERIOR AND SOLEUS

Muscles	Contraction Times (ms)
Tibialis Anterior [24], [25]	[47,134]
Soleus [26]	[127.1, 185.9]

D. Activation Dynamics of Motor Units

The contraction times (t_{peak}) were calculated by linearly mapping from fast to slow motor neurons based on the range specified in Table I. The peak amplitudes (A_{peak}) were specified between 0.1 and 1. A_{peak} was normalized using the number of MU spike trains.

The motor-unit twitch in response to an action potential in the associated motoneuron was modeled as the Fuglevand model [27]. The Fuglevand model uses a set of differential equations to describe the activation and force generation of motor units. It assumes that each motor unit has a specific activation threshold, which determines the level of input required to activate it, and that the motor units are recruited in order of size based on the size principle. The contraction times, peak amplitudes, and spike trains were substituted in the discrete-time equation 3 of the Fuglevand model as stated by Cisi et.al., [28].

$$f(n) = 2e^{\frac{-T}{t_{peak}}} f(n-1) - exp(\frac{-2T}{t_{peak}}) f(n-2) + \frac{A_{peak} T^2}{t_{peak}} exp(1 - \frac{T}{t_{peak}}) e(n-1) \quad (3)$$

where T = $\frac{1}{fs}$, fs is the sampling frequency, t_{peak} is the contraction time, A_{peak} is the peak amplitude, e(n) is the value of spike train.

The activation profiles (f(n)) were mapped to the maximum AD of EMG data for better analysis and stored as activation dynamics of motor units in the form of time series for joint torque and stiffness estimation.

After decomposing motor units and finding the activation profiles of those motor units, the data such as angles and torque from the Achilles, the activation profiles of EMG envelopes, and the activation profiles of motor units were stored as time series for further estimation.

The schematic diagram of Subsections II-B, II-C and II-D were described in Figure 8.

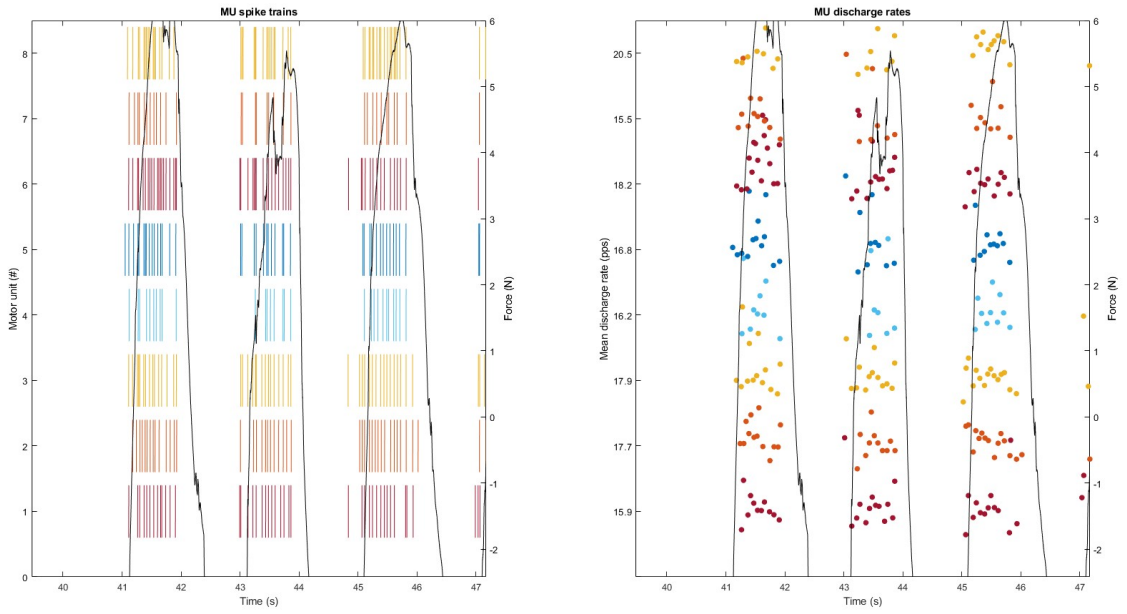

Fig. 5: Spike Trains and Discharge Rate of Tibialis Anterior with torque data

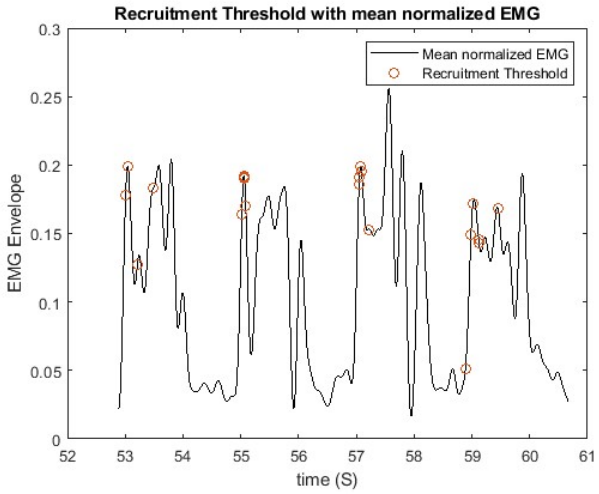

Fig. 6: Recruitment Threshold of Tibialis Anterior

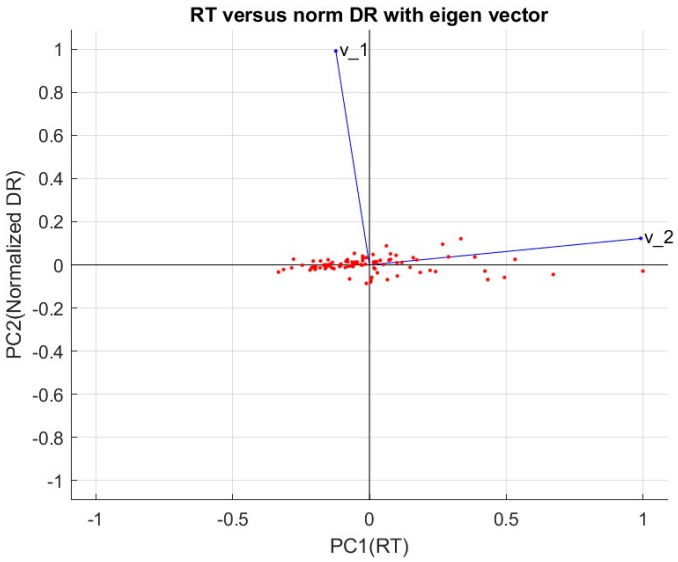

Fig. 7: Principal Component Analysis of Tibialis Anterior. Each point of the scatter plot represents a measurement (discharge rate and recruitment threshold) of a single motor unit (MU).

E. Stiffness Estimation using System Identification

The first and last three seconds of all the data were removed to avoid transition effects. To estimate joint stiffness using a system identification technique, an extended multisegment (MS) algorithm has been designed to combine ensemble- with time-averaging to analyze time-varying properties [5]. The torque and position signals were segmented into a certain number of sinusoidal realizations. The total number of realizations (nr) in each 2-minute trial depended on the initial sine frequency (f) and the time stamps ([t1 t2]).

$$nr = (t2 - t1) * f - 2$$

To segment position, torque, and perturbation signals into separate realizations, torque minimum peaks were determined. Peak-to-peak data constituted a single realization; however, due to the variability caused by the subject's voluntary behavior, the length of each

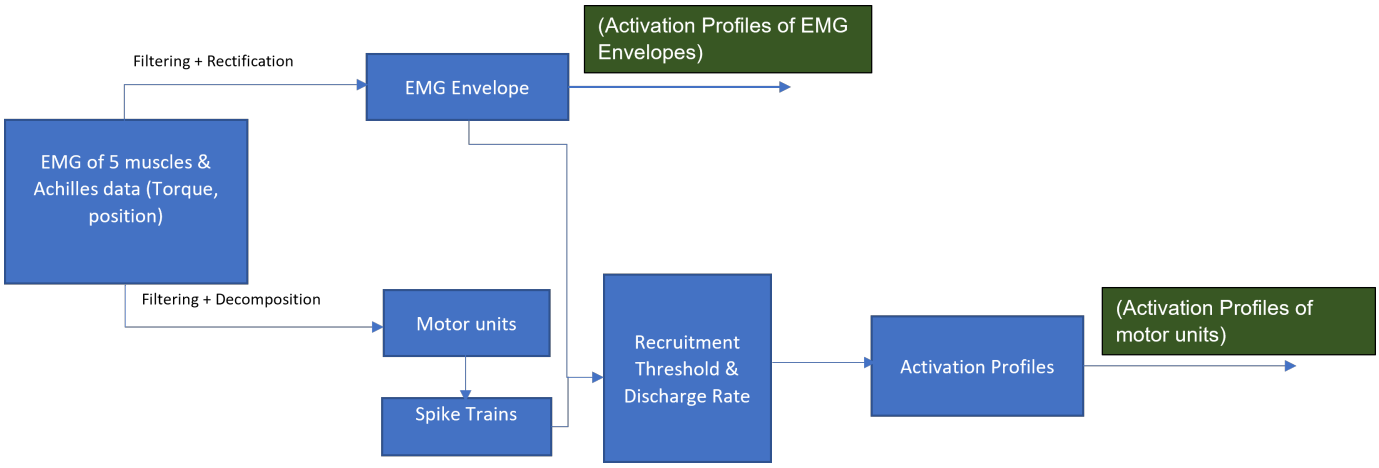

Fig. 8: Schematic Diagram of determining Activation Dynamics of EMG Envelopes and individual motor units. A detailed explanation of the steps involved is explained in steps 1,2 of Figure 27

.

realization was different. Therefore, realizations were re-sampled via interpolation to have an equal number of samples, corresponding to the samples in one period at the Achilles sampling rate (2048 Hz). The realizations were aligned and the outliers were removed to reduce variability among them and the ensemble mean was removed to amplify the perturbation-induced response. The MS algorithm computes double-sided estimates of the impulse response function (IRF) of the system by means of auto and cross-correlation functions. The IRFs were integrated to estimate the stiffness. These steps are described in detail in previous studies [29]. The statistical validity of the MS algorithm was evaluated using a bootstrapping approach. This involved randomly selecting 95% of the realizations from the ensemble to calculate the stiffness estimate, and this was repeated 35 times to find the mean of the estimated stiffness. After manual inspection of the estimated stiffness of each subject, it was concluded to use a moving median filter and moving mean filter with a window of five samples. The mean of joint stiffness estimated using the system identification technique for all the subjects is shown in Figure 9. These stiffness data were stored as time series for further processing.

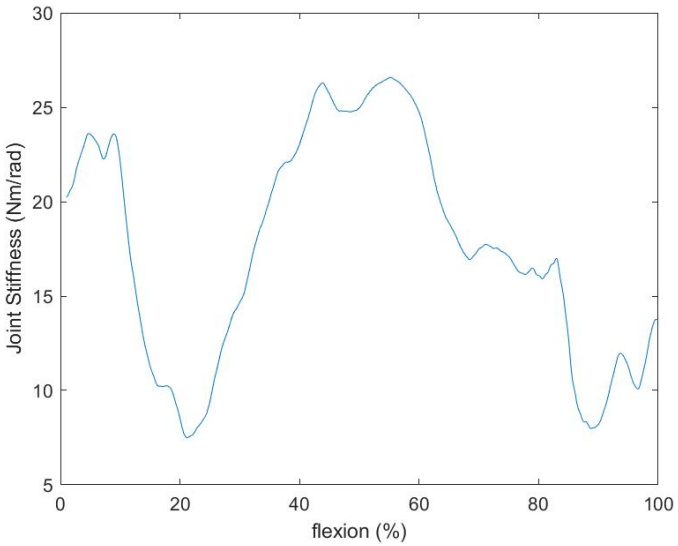

Fig. 9: Mean of reference joint stiffness of all the subjects identified using System Identification

F. Stiffness Estimation using EMG-driven musculoskeletal modeling

The next step of this study was the identification of the joint stiffness using Calibrated EMG-Informed Neuromusculoskeletal Modelling (CEINMS). The torque and the angle data were segmented by finding the minimum peaks. The data such as torque, angle, stiffness, activation dynamics of EMG envelopes, and activation dynamics of motor units were normalized to the length of 1000 for calibration. Later, the means of all these data were determined and stored as time series for further analysis. These mean data were used as calibration data while the entire 40 seconds of data stored from Subsections II-D and II-B3 were used for execution.

The OpenSim software [30], which is open-source, was used to scale the model based on the shape factors calculated manually for each subject's femur, tibia, and foot. This scaled model was optimized by changing the muscle parameters of the entire lower limb based on a generic model [31].

The Calibrated EMG-Informed Neuromusculoskeletal Modelling (CEINMS) toolbox [18], also open-source,

was used to estimate ankle torque, stiffness, and forces of MTUs based on recorded EMGs, joint angles, torques, and the optimized scaled OpenSim model. The model developed by Cop et al. estimates the stiffness of muscle fibers and tendons at the MTU level and then projects it to the joint level [9] as shown in Figure 10. A brief explanation of the model adapted from [9] is described below.

The input EMG and motor unit activations (u) were mapped to *MTU activations* (a) based on the equation:

$$a = \frac{e^{Au} - 1}{e^{A} - 1} \tag{4}$$

where A is the shape factor.

The ankle angle data from the Achilles were mapped to *MTU moment arms* (r_i) and *MTU forces* are calculated as a function of the maximum isometric force of the muscle, active force-length, force-velocity, and passive force-length relationships, normalized length, velocity and pennation angle of the muscle fiber.

$$F^{MTU} = F^{max}(af_a(l^m)f_v(v^m) + f_p(l^m) + v^m d)cos\Phi \tag{5}$$

As the next step, *MTU stiffness* is calculated as:

$$K^{MTU} = (K_{eq}^{m^{-1}} + K^{t^{-1}})^{-1} \tag{6}$$

where K_{eq}^{m} is the equivalent stiffness of muscle fiber as a function of muscle force and length along the direction of the tendon's line of action, and K_t is the stiffness of the tendon as a function of tendon force and length. The computational formula of these terms is detailed by Cop et al. [9].

The projection of the MTU forces to obtain *joint torque* was done using Equation 7

$$\tau = \sum_{i=1}^{mtu}(F_i^{MTU} r_i) \tag{7}$$

Simultaneously, the projection of MTU forces and stiffness to obtain *joint stiffness* was done using Equation 8

$$K^J = \sum_{i=1}^{mtu}(K_i^{MTU} r_i^2 - \frac{\partial r_i}{\partial \theta} F_i^{MTU}) \tag{8}$$

Two different models were calibrated using calibration data of EMG envelopes and motor units, respectively. The parameters such as Tendon Slack Length (TSL), Optimal Fiber Length (OFL), strength coefficients, and shape factors were used for calibration. For calibration using EMG Envelopes, the mean of normalized torque, angle, AD of EMG envelopes, and stiffness were used for calibration while for motor units, the mean of normalized torque, angle, AD of motor units, and stiffness was used. These calibration data were the respective mean of all the aforementioned data across all repetitions per subject.

During the model calibration processes, parameters such as optimal fiber length, tendon slack length, maximum isometric force, and shape factor were adjusted to best fit the input reference joint torque and stiffness. Also, a certain range was specified for the optimal fiber length and tendon slack length (usually the range is limited to vary 5% of their initial value) [9]. The calibration aimed to find the optimal model parameter set that minimizes the error between the reference and computed values [7]. An objective function (Equation: 9) is used to perform the model calibration at the torque and stiffness levels simultaneously.

$$F_{obj} = avg(\alpha E_\tau + \beta E_{k^J} + p) \tag{9}$$

where, E_τ,E_{k^J} are the normalized differences of estimated joint torque and stiffness while α,β are the weights of the contribution of torque and stiffness that can be altered to obtain a better fit [9].

The calibrations were followed by the actual executions using the entire 40 seconds of experimental data of each trial for each model respectively (8 trials per subject; 16 executions for two models). The inputs for both the model executions included commonly the calibrated subject data together with the 40 seconds data of torque, angle with AD of EMG, and AD of motor units respectively. The two models' respective torque and stiffness results were stored for further validation.

G. Data Validation

The validation of the proposed frameworks (Model with AD of EMG Envelopes and Model with AD of motor units) was performed against the results of System identification and experimental data. The model driven by the AD of EMG envelopes and the model driven by the AD of motor units were validated using the torques and the stiffness values. The reference data for validation at the torque level are the experimental torque measured by Achilles and at the stiffness level the joint stiffness obtained using the system identification technique. The modeled data are the torque and stiffness output from CEINMS. The reference data were also the data used for calibrating the models.

At the torque level, the modeled torque data were compared to reference torque data, and both their shapes and magnitudes were evaluated using the coefficient of determination (R^2) and the Root Mean Squared Error

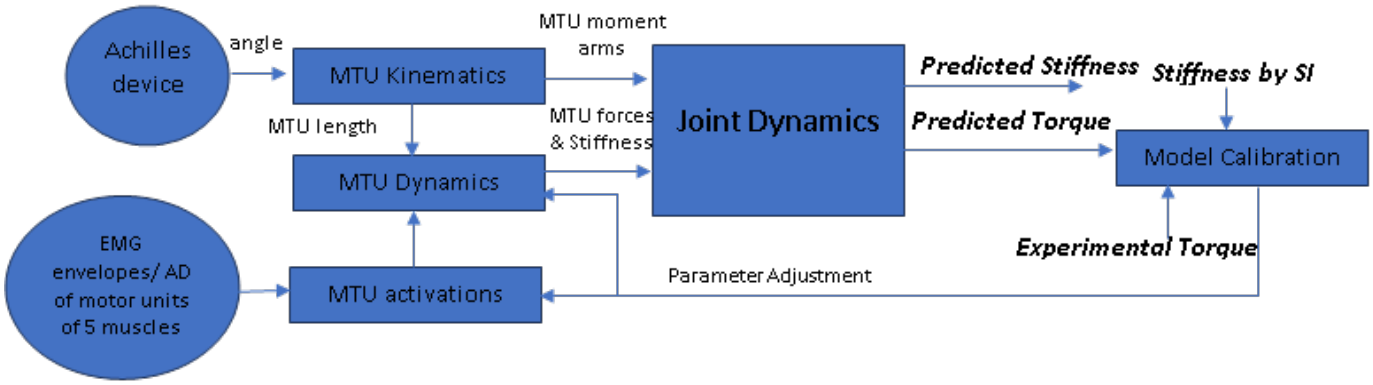

Fig. 10: Schematic diagram of the EMG-driven musculoskeletal model that estimates the stiffness of muscle fibers and tendons at the MTU level and then projects it to the joint level. Figure adapted from [8]. A more detailed version can be found in [9].

(RMSE). Further, the RMSE values were normalized (nRMSE) using the root mean square of the experimental data.

Similarly, the modeled stiffness were compared to the reference stiffness, and the results were assessed in shape and magnitude by the R^2, RMSE, and nRMSE.

The schematic diagram of Subsections II-E, II-F and II-G were described in Figure 11.

III. Results

The activation dynamics of the EMG Envelope to drive the model was found using the steps provided in Subsection II-B3. The result of the mean normalized EMG Envelope of TA, GM, GL, and PL against the torque is shown in Figure 12.

The activation dynamics of the motor units decomposed in Subsection II-C were found using the steps provided in Subsection II-D. The mean discharge rates, recruitment thresholds, peak amplitudes, and contraction times of TA found in this study are displayed in table II.

TABLE II: MEANS (AND STD.) OF DISCHARGE RATES, RECRUITMENT THRESHOLD, PEAK AMPLITUDE, AND CONTRACTION TIMES OF TIBIALIS ANTERIOR

Subject	DR (Hz)	RT	t_{peak} (ms)	A_{peak}
1	10.65 (1.76)	0.04 (0.01)	0.05 (0.001)	0.13 (0.02)
2	13.17 (1.79)	0.06 (0.02)	0.05 (0.002)	0.15 (0.02)
3	16.56 (1.69)	0.18 (0.03)	0.05 (0.002)	0.14 (0.02)
4	14.16 (2.59)	0.09 (0.04)	0.05 (0.003)	0.14 (0.03)
5	12 (1.58)	0.09 (0.03)	0.05 (0.001)	0.14 (0.02)
6	12.07 (1.78)	0.25 (0.19)	0.05 (0.002)	0.16 (0.02)

The result of the activation profile of the motor units and EMG Envelope of TA against the torque is shown in Figure 13.

Both Figures 12 and 13 show that the muscles TA, GM, GL, and PL lie in their respective flexion and proved that the activation dynamics found can be used to drive the model. On the contrary, from Figure 14, it was evident that the EMG envelope of Soleus lies in the dorsi flexion instead of plantar flexion. Moreover, the motor units decomposed from Soleus were too few compared to Tibialis Anterior. So, the data derived from the channels corresponding to the Soleus muscle were not useful for further estimation.

For all the trials of all the subjects (48 trials in total), the estimated torques of the model obtained using AD of EMG envelopes were compared to the experimental torques obtained from Achilles as shown in Figure 15. R^2 values ranged from 0.13-0.60 (mean - 0.42; standard deviation - 0.04). RMSE values ranged from 2.94 Nm-13.66 Nm (mean - 5.98 Nm; standard deviation - 1.02). nRMSE values ranged from 0.57-2.97 (mean - 1.38; standard deviation - 0.23).

On the other hand, the estimated torques of the model obtained using AD of motor units were compared to the experimental torques obtained from Achilles as shown in Figure 15. R^2 values ranged from 0.60-0.82 (mean - 0.70; standard deviation - 0.02). RMSE values ranged from 1.85 Nm-3.56 Nm (mean - 2.70 Nm; standard deviation - 0.37). nRMSE values ranged from 0.47-0.77 (mean - 0.62; standard deviation - 0.08). The values of both methods are given in Figures 17, 18, 19.

At the stiffness level, the joint stiffness estimated by the model obtained using AD of EMG envelopes was compared to the stiffness obtained using the system identification technique as shown in Figure 16. R^2 values ranged from 0.04-0.35 (mean - 0.13; standard deviation - 0.04). RMSE values ranged from 6.16 Nm/rad-24.72 Nm/rad (mean - 15.53 Nm/rad; standard deviation - 2.56). nRMSE values ranged from 0.49-1.14 (mean -

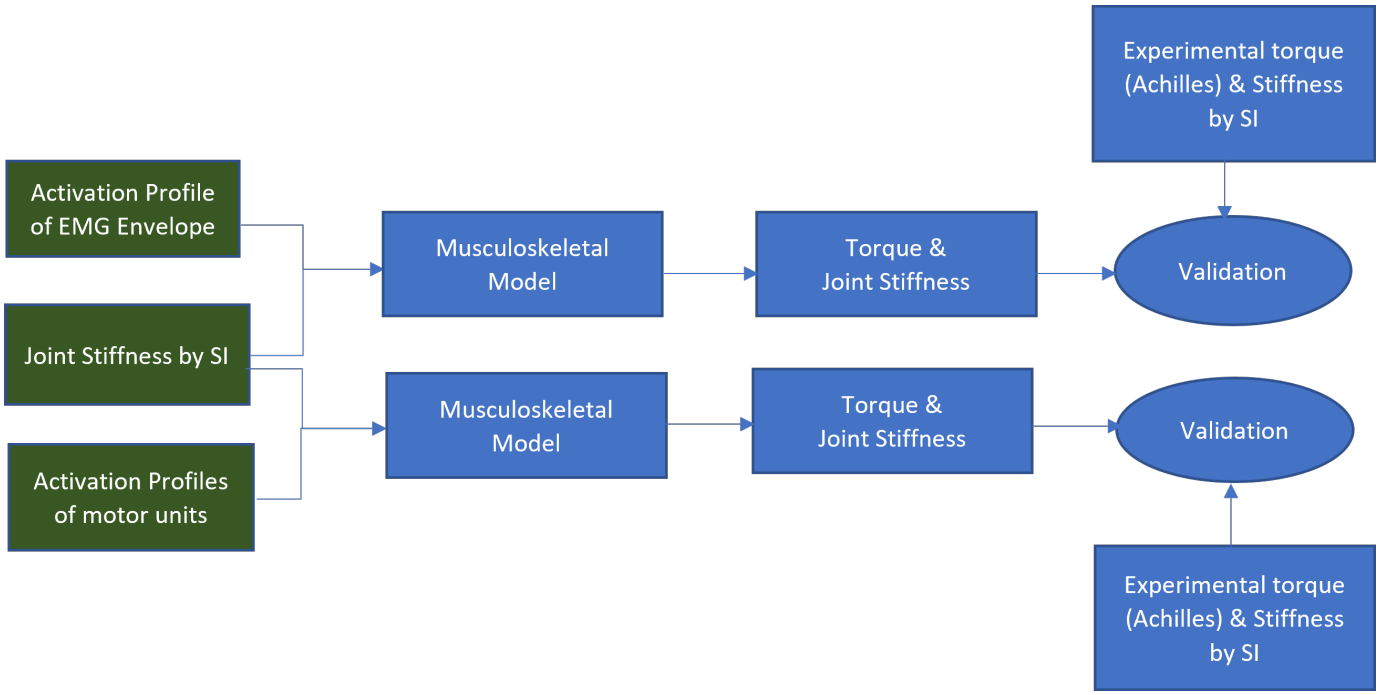

Fig. 11: Schematic Diagram of determining the torque and stiffness using the musculoskeletal model. The working of the musculoskeletal model is explained in Figure 10. A detailed explanation of the steps involved is explained in step 3,4,5 of Figure 27

.

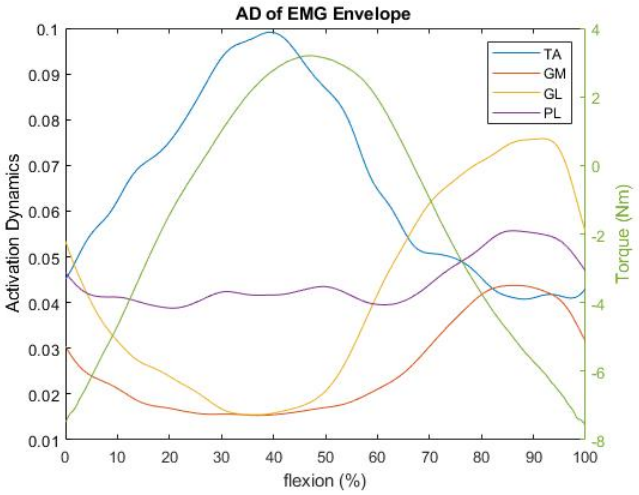

Fig. 12: Plot of the mean of AD of EMG envelopes and torques of Tibialis Anterior, Gastrocnemius medialis, Gastrocnemius lateralis, and Peroneus longus of all trials of all subjects

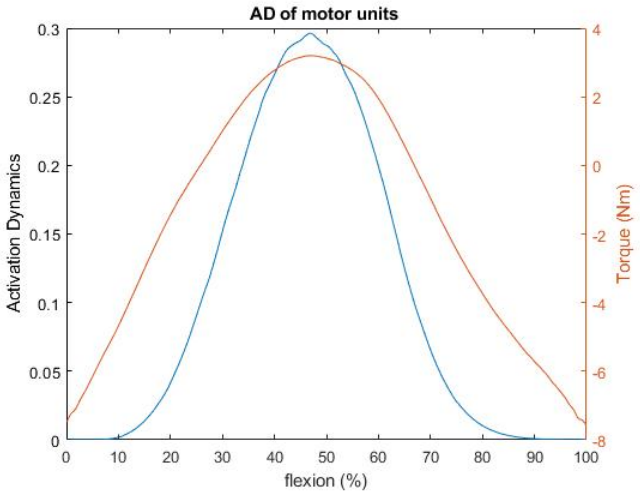

Fig. 13: Plot of mean activation dynamics of motor units and torque of Tibialis Anterior for all trials of all subjects

0.78; standard deviation - 0.15).

On the other hand, the estimated stiffness of the model obtained using AD of motor units was compared to the stiffness obtained using the system identification technique as shown in Figure 16. R^2 values ranged from 0.03-0.36 (mean - 0.17; standard deviation - 0.04). RMSE values ranged from 8.58 Nm/rad-23.06 Nm/rad (mean - 16.34 Nm/rad; standard deviation - 3.07). nRMSE values ranged from 0.64-1.12 (mean - 0.83; standard deviation - 0.18). The values of both methods are given in Figures 17, 18, 19.

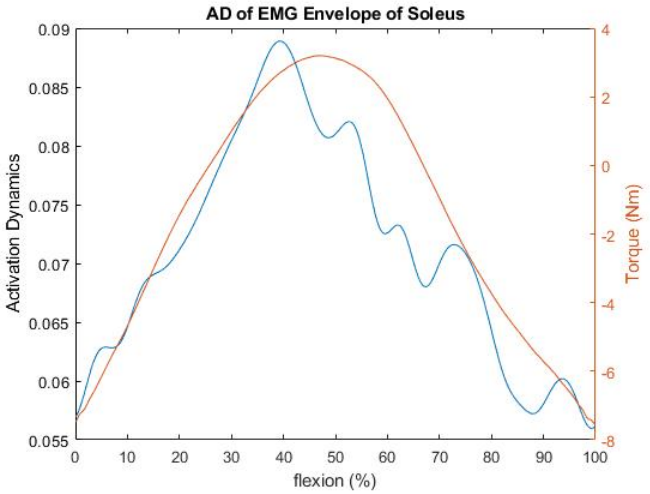

Fig. 14: Plot of mean activation dynamics of EMG envelope and torque of Soleus for all trials of all subjects

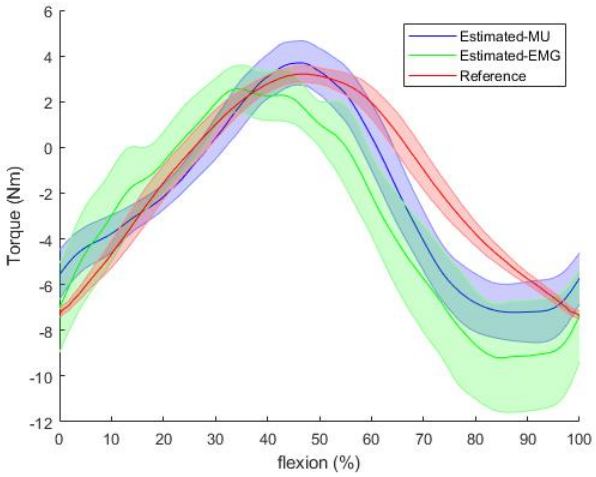

Fig. 15: Comparison of the torque estimations using AD of EMG envelopes and motor units against Achilles data

IV. Discussion

In this study, a neuromusculoskeletal framework driven by the identification of motoneuron properties and a musculoskeletal framework driven by EMG envelopes were developed and validated using the experimental results and results of system identification methods.

First, some observations and results obtained during this project were analyzed followed by detailed answers to the main research questions presented in Section I, difficulties encountered during the study, limitations, and future works.

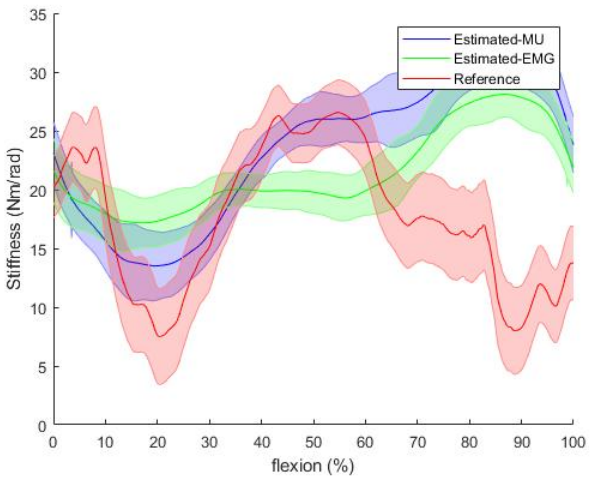

Fig. 16: Comparison of the stiffness estimations using AD of EMG envelopes and motor units against system identification

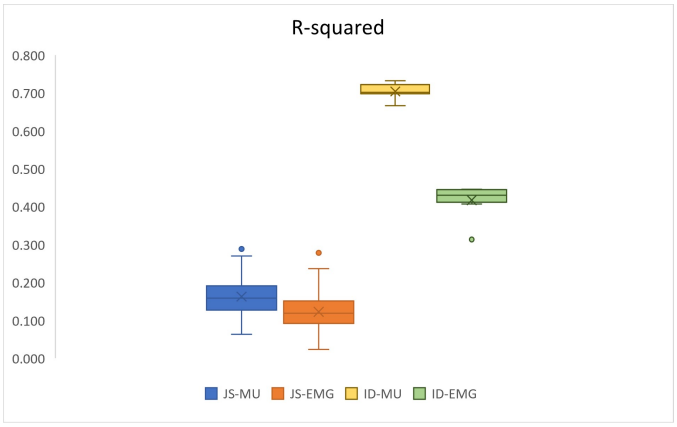

Fig. 17: Box Plot of R-squared values of Joint Stiffness and torque estimated using the model driven by MU and EMG

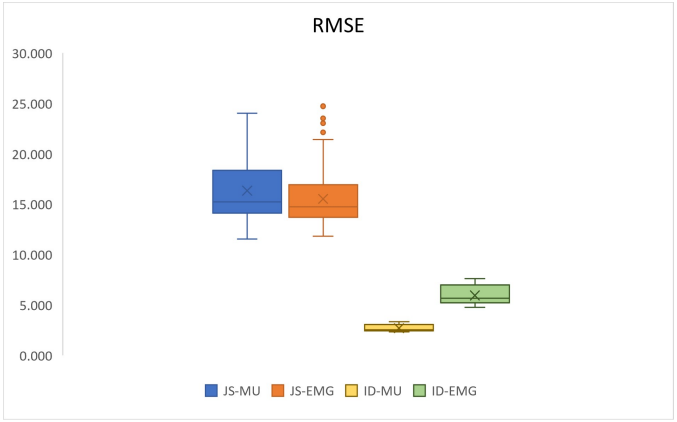

Fig. 18: Box Plot of Root Mean Square Error values of Joint Stiffness and torque estimated using the model driven by MU and EMG

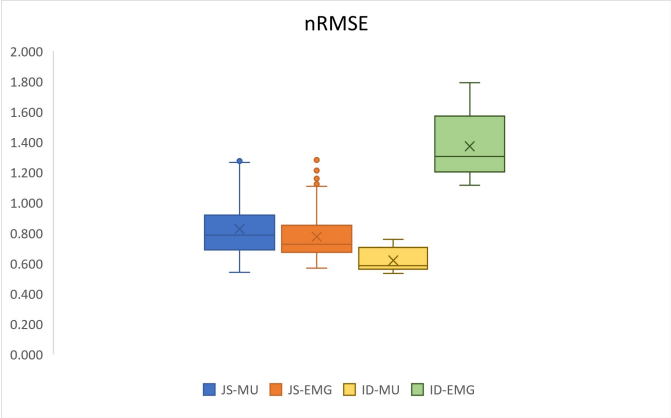

Fig. 19: Box Plot of normalized Root Mean Square Error values of Joint Stiffness and torque estimated using the model driven by MU and EMG

A. *Observations and Discussion of Results*

The values and the graphs of Section III explain the results obtained using the activation dynamics of EMG envelopes, and activation dynamics of motor units. Among several outputs of the model, the torque and stiffness were used for validation.

The validation of the motor unit-driven musculoskeletal model at the torque level showed that the model had lower nRMSE and higher co-efficient of correlation (R-squared) (Figure 19,17) than the EMG-driven musculoskeletal model making the later better at prediction of torque. This result was in line with the findings of Gogeascoechea et al., that the activation dynamics of motor units had higher similarity to the torque profiles [22]. By modeling the activation of motor units, the model could more accurately represent the muscle activation patterns, which could lead to more accurate torque estimates as motor units are the fundamental building blocks of muscle activation, and the activation of each motor unit contributes to the overall force and torque generated by the muscle. A limitation of decomposing the motor units is that the smaller MUs with lower action potentials may not be decomposed in the presence of bigger MUs with higher action potentials [20]. As the smaller MUs are recruited first, the estimated results could have a negative effect. Moreover, the MTU dynamics block of Figure 10 uses a Hill-type muscle model to estimate MTU forces. The effect of activation on the Hill-type muscle model is typically modeled using a muscle activation function (Equation 4), which describes how the muscle activation level varies over time. The motor units have a higher level of activation profile than EMG Envelopes (Refer Figure 13) which could also be one of the reasons for better estimation of torque by the model driven by AD of motor units.

For the validation at the stiffness level, as there is no golden standard, the stiffness values obtained using the model were compared to previous studies. Lee et al., stated ankle stiffness between 30 Nm/rad and 60 Nm/rad for various gait conditions [32] and Cop et al., reported values from 5 Nm/rad to 30 Nm/rad [8]. The works of Moya-Esteban et al. estimated the stiffness to be between 5 Nm/rad and 45 Nm/rad under dynamic conditions and between 0 Nm/rad and 50 Nm/rad under static condition [5]. The values of this study were roughly between 7 Nm/rad and 40 Nm/rad. Even if the predicted results of the model were not satisfied with the system identification results, the estimation was comparable to the previous studies. During the model calibration, the model uses the torque and stiffness values based on the weights assigned to them as stated in Equation 9 [9]. The stiffness estimation had no significant difference irrespective of the weights assigned to torque and stiffness during calibration.

Overall, it was evident that the torque estimation of the model was better when it was driven by the activation dynamics of the motor units than the activation dynamics of EMG envelopes while it was vice-versa for stiffness estimation. The hypothesis of the entire research that the comprehensive neuromusculoskeletal framework that combines stiffness estimation and the identification of motoneuron properties will improve the estimation of joint torque was proved. But the prediction of joint stiffness was worse.

Though the variations between both models are very few, the overall prediction of stiffness is worse than torque estimations. This might be due to the large fluctuations in the stiffness estimated through the system identification technique even after filtering. The stiffness estimated by both models showed worse estimations in plantar flexion. This could be because only muscles with bi-polar EMG data were used to drive plantar flexion. Though the prediction of dorsi flexion was better in the model driven by motor units, due to a very bad prediction of plantar flexion, the RMSE was large than EMG driven model.

B. *Practical difficulties*

Firstly, the Signal-to-Noise Ratios (SNRs) were calculated and the channels above SNR threshold $>$ 1.8dB [33] were chosen for further processing. But this led to the elimination of many trials and the decomposition was better even with the channels of SNR$>$1.8dB. So, it is still unclear if the quality of the EMG data used is good. Secondly, the Soleus muscle EMG signals recorded from channels 65 to 128 were too noisy and their removal led

to the exclusion of certain trials or subjects. Additionally, compared to Tibialis Anterior, fewer motor units were identified from Soleus, and its EMG envelope showed dorsi flexion instead of plantar flexion. Consequently, the data from Soleus was considered unsuitable for estimation. As Gastrocnemius Medialis had very small values compared to Gastrocnemius Lateralis, Soleus was replaced with data from GL in the model. The cause of this problem was found to be a normalization setting in REFA that averaged all values from 128 channels over the entire data. So, the data of TA were also affected by Soleus.

Thirdly, while calibrating the model with the average of the experimental data, the margins of the parameters such as TSL and OFL need to be specified. It was found that the higher the margin, the better the calibration was performed. With the limits of [parameters+(parameters·0.3), parameters-(parameters·0.3)] showed improved calibration results than [parameters+(parameters·0.15), parameters-(parameters·0.15)] and [parameters+(parameters·0.05), parameters-(parameters·0.05)]

C. Limitations and future work

This study has certain limitations that can be improved during further research. Only five muscles were included and Soleus was dropped in between due to the aforementioned reasons. As a result, the Soleus was driven by gastrocnemius lateralis which might have affected the results of the model. The twitch methodology used to decompose the motor units lacks validation against actual twitches. The subject might only be recruiting slow MU types as there are not enough data to pool all types of motor units. Further, the force profile is usually used to identify the recruitment threshold. But in this study, EMG Envelopes were used as the MVC data is relatively low compared to the MVC data obtained using other dynamometers such as Biodex. The MVC data in the previous works were up to 40 Hz [34] while here it was only a maximum of 5 Hz. The actual data from Achilles had low activation levels causing a limitation in the use of PCA as larger motor units usually have better PCA. In this study, very few data points were used leading to the recruitment of only a subset of the entire population. The actual mapping of the principal component includes both slow and fast MUs while in this study the slow MUs were mapped to both conditions. The stiffness data of system identification contained noise/fluctuations which even after filtering was not satisfactory. The EMG data from the channels had noises that probably correlated with the adjacent channels. As this study clearly explains that a model driven by activation dynamics of motor units is better in torque estimation, further research can be directed towards improving the results of stiffness estimation by including better quality EMG signals to identify the motor units and activation dynamics. By doing so, the plantar flexion can be driven by the soleus data obtained using a mono-polar electrode rather than the data from the bipolar electrode. This might have had a huge impact on the results as the mono-polar electrode channels are considered to provide large amplitude and stronger signals than the bi-polar channels [35]. Mono-polar EMG electrodes have a larger surface area and can capture electrical activity from a larger area of the muscle, which results in a stronger signal. In this study, only one MVC was performed per subject. In the future, multiple trials of MVC should be performed to obtain higher MVC data with perturbation using Achilles. Since only the isometric condition is taken into account in this study, further analysis can be done under dynamic conditions. This study does not include SRS that appears only during isometric conditions when the movement of filaments in the sarcomere stops [36].

REFERENCES

[1] M. Sartori, M. Maculan, C. Pizzolato, M. Reggiani, and D. Farina, "Modeling and simulating the neuromuscular mechanisms regulating ankle and knee joint stiffness during human locomotion." *Journal of neurophysiology*, vol. 114, no. 4, pp. 2509–27, 10 2015.

[2] E. J. Rouse, R. D. Gregg, L. J. Hargrove, and J. W. Sensinger, "The Difference Between Stiffness and Quasi-Stiffness in the Context of Biomechanical Modeling," *IEEE Transactions on Biomedical Engineering*, vol. 60, no. 2, pp. 562–568, 2 2013.

[3] R. M. Sigrist, J. Liau, A. E. Kaffas, M. C. Chammas, and J. K. Willmann, "Ultrasound Elastography: Review of Techniques and Clinical Applications," *Theranostics*, vol. 7, no. 5, pp. 1303–1329, 2017.

[4] M. van de Ruit, W. Mugge, G. Cavallo, J. Lataire, D. Ludvig, and A. C. Schouten, "Quantitative comparison of time-varying system identification methods to describe human joint impedance," *Annual Reviews in Control*, vol. 52, pp. 91–107, 2021.

[5] A. M. Esteban, R. C. van 't Veld, C. P. Cop, G. Durandau, M. Sartori, and A. C. Schouten, "Estimation of Time-Varying Ankle Joint Stiffness Under Dynamic Conditions via System Identification Techniques," in *2019 41st Annual International Conference of the IEEE Engineering in Medicine and Biology Society (EMBC)*. IEEE, 7 2019, pp. 2119–2122.

[6] D. Ludvig and E. J. Perreault, "System identification of physiological systems using short data segments," *IEEE Transactions on Biomedical Engineering*, vol. 59, no. 12, pp. 3541–3549, 2012.

[7] M. Sartori, M. Reggiani, D. Farina, and D. G. Lloyd, "EMG-Driven Forward-Dynamic Estimation of Muscle Force and Joint Moment about Multiple Degrees of Freedom in the Human Lower Extremity," *PLoS ONE*, vol. 7, no. 12, p. e52618, 12 2012.

[8] C. P. Cop, G. Durandau, A. M. Esteban, R. C. van 't Veld, A. C. Schouten, and M. Sartori, "Model-Based Estimation of Ankle Joint Stiffness During Dynamic Tasks: a Validation-Based Approach," in *2019 41st Annual International Conference of the IEEE Engineering in Medicine and Biology Society (EMBC)*. IEEE, 7 2019, pp. 4104–4107.

[9] C. P. Cop, A. C. Schouten, B. Koopman, and M. Sartori, "Electromyography-driven model-based estimation of ankle torque and stiffness during dynamic joint rotations in perturbed and unperturbed conditions," *Journal of Biomechanics*, vol. 145, p. 111383, 12 2022.

[10] J. M. Wakeling, S. S. M. Lee, A. S. Arnold, M. de Boef Miara, and A. A. Biewener, "A Muscle's Force Depends on the Recruitment Patterns of Its Fibers," *Annals of Biomedical Engineering*, vol. 40, no. 8, pp. 1708–1720, 8 2012.

[11] C. P. Cop, G. Cavallo, R. C. van'T Veld, B. F. Koopman, J. Lataire, A. C. Schouten, and M. Sartori, "Unifying system identification and biomechanical formulations for the estimation of muscle, tendon and joint stiffness during human movement," 7 2021.

[12] N. Garg, S. B. Park, S. Vucic, C. Yiannikas, J. Spies, J. Howells, W. Huynh, J. M. Matamala, A. V. Krishnan, J. D. Pollard, D. R. Cornblath, M. M. Reilly, and M. C. Kiernan, "Differentiating lower motor neuron syndromes," *Journal of Neurology, Neurosurgery & Psychiatry*, vol. 88, no. 6, pp. 474–483, 6 2017.

[13] F. Buchthal and H. Schmalbruch, "Motor unit of mammalian muscle." *Physiological Reviews*, vol. 60, no. 1, pp. 90–142, 1 1980.

[14] R. E. Sica and A. J. McComas, "Fast and slow twitch units in a human muscle." *Journal of neurology, neurosurgery, and psychiatry*, vol. 34, no. 2, pp. 113–120, 1971.

[15] A. G. Hernandez, R. O. Kobayashi, U. S. Yavuz, and M. Sartori, "Identification of Motor Unit Twitch Properties in the Intact Human in Vivo," in *Proceedings of the Annual International Conference of the IEEE Engineering in Medicine and Biology Society, EMBS*. Institute of Electrical and Electronics Engineers Inc., 2021, pp. 6310–6313.

[16] I. Campanini, A. Merlo, and D. Farina, "Motor unit discharge pattern and conduction velocity in patients with upper motor neuron syndrome," *Journal of Electromyography and Kinesiology*, vol. 19, no. 1, pp. 22–29, 2 2009.

[17] F. Negro, S. Muceli, A. M. Castronovo, A. Holobar, and D. Farina, "Multi-channel intramuscular and surface EMG decomposition by convolutive blind source separation," *Journal of Neural Engineering*, vol. 13, no. 2, 2 2016.

[18] C. Pizzolato, D. G. Lloyd, M. Sartori, E. Ceseracciu, T. F. Besier, B. J. Fregly, and M. Reggiani, "CEINMS: A toolbox to investigate the influence of different neural control solutions on the prediction of muscle excitation and joint moments during dynamic motor tasks," *Journal of Biomechanics*, vol. 48, no. 14, pp. 3929–3936, 11 2015.

[19] The MathWorks Inc., "Matlab," Natick, Massachusetts, United States, 2022.

[20] A. Holobar and D. Zazula, "Multichannel blind source separation using convolution Kernel compensation," *IEEE Transactions on Signal Processing*, vol. 55, no. 9, pp. 4487–4496, 9 2007.

[21] A. Holobar, M. A. Minetto, and D. Farina, "Accurate identification of motor unit discharge patterns from high-density surface EMG and validation with a novel signal-based performance metric," *Journal of Neural Engineering*, vol. 11, no. 1, 2 2014.

[22] A. Gogeascoechea, A. Kuck, E. van Asseldonk, F. Negro, J. R. Buitenweg, U. S. Yavuz, and M. Sartori, "Interfacing With Alpha Motor Neurons in Spinal Cord Injury Patients Receiving Trans-spinal Electrical Stimulation," *Frontiers in Neurology*, vol. 11, 6 2020.

[23] H. Gray, *Anatomy*, 30th ed. Philadelphia, PA: Lea & Febiger, 6 1985.

[24] M. R. Roos, C. L. Rice, D. M. Connelly, and A. A. Vandervoort, "Quadriceps muscle strength, contractile properties, and motor unit firing rates in young and old men." *Muscle & nerve*, vol. 22, no. 8, pp. 1094–103, 8 1999.

[25] S. Andreassen and L. Arendt-Nielsen, "Muscle fibre conduction velocity in motor units of the human anterior tibial muscle: a new size principle parameter." *The Journal of Physiology*, vol. 391, no. 1, pp. 561–571, 10 1987.

[26] A. A. Vandervoort and A. J. McComas, "A comparison of the contractile properties of the human gastrocnemius and soleus muscles," *European Journal of Applied Physiology and Occupational Physiology*, vol. 51, no. 3, pp. 435–440, 9 1983.

[27] A. J. Fuglevand, D. A. Winter, and A. E. Patla, "Models of recruitment and rate coding organization in motor-unit pools," *Journal of Neurophysiology*, vol. 70, no. 6, pp. 2470–2488, 12 1993.

[28] R. R. L. Cisi and A. F. Kohn, "Simulation system of spinal cord motor nuclei and associated nerves and muscles, in a Web-based architecture," *Journal of Computational Neuroscience*, vol. 25, no. 3, pp. 520–542, 12 2008.

[29] D. Ludvig, M. Plocharski, P. Plocharski, and E. J. Perreault, "Mechanisms contributing to reduced knee stiffness during movement," *Experimental Brain Research*, vol. 235, no. 10, pp. 2959–2970, 10 2017.

[30] S. L. Delp, F. C. Anderson, A. S. Arnold, P. Loan, A. Habib, C. T. John, E. Guendelman, and D. G. Thelen, "OpenSim: Open-Source Software to Create and Analyze Dynamic Simulations of Movement," *IEEE Transactions on Biomedical Engineering*, vol. 54, no. 11, pp. 1940–1950, 11 2007.

[31] L. Modenese, E. Ceseracciu, M. Reggiani, and D. G. Lloyd, "Estimation of musculotendon parameters for scaled and subject specific musculoskeletal models using an optimization technique," *Journal of biomechanics*, vol. 49, no. 2, pp. 141–148, 2016.

[32] H. Lee and N. Hogan, "Time-Varying Ankle Mechanical Impedance During Human Locomotion," *IEEE Transactions on Neural Systems and Rehabilitation Engineering*, vol. 23, no. 5, pp. 755–764, 9 2015.

[33] A. Phinyomark, C. Limsakul, P. Phukpattaranont, and P. Phukpattaranont, "EMG Feature Extraction for Tolerance of White Gaussian Noise Evidence informed methods for predicting rehabilitation outcomes in patellofemoral pain View project Myoelectric Control View project INTERNATIONAL WORKSHOP AND SYMPOSIUM ON SCIENCE AND TECHNOLOGY 2008 I-SEEC 2008-178-EMG feature extraction for tolerance of white Gaussian noise," Tech. Rep., 2008. [Online]. Available: https://www.researchgate.net/publication/263765853

[34] D. M. Connelly, C. L. Rice, M. R. Roos, and A. A. Vandervoort, "Motor unit firing rates and contractile properties in tibialis anterior of young and old men," *Journal of Applied Physiology*, vol. 87, no. 2, pp. 843–852, 8 1999.

[35] M. Mohr, T. Schön, V. von Tscharner, and B. M. Nigg, "Intermuscular Coherence Between Surface EMG Signals Is Higher for Monopolar Compared to Bipolar Electrode Configurations," *Frontiers in Physiology*, vol. 9, 5 2018.

[36] L. Cui, E. J. Perreault, H. Maas, and T. G. Sandercock, "Modeling short-range stiffness of feline lower hindlimb muscles," *Journal of Biomechanics*, vol. 41, no. 9, pp. 1945–1952, 2008.

V. Acknowledgement

The author would like to thank all the supervisors involved in the project (Massimo Sartori, Utku Yavuz,

Pablo Cop and Antonio de Jesus Gogeascoechea Hernandez) for sharing their valuable feedback which was very useful for this research and thanks to Alejandro Moya Esteban for the framework of stiffness estimation using system identification without which this research would not have been possible. Last but not least, a special thanks to Pablo and Antonio who acquired the data used in this study prior to commencing this research and provided constant support, feedback and encouragement which was a driving force throughout this study.

APPENDIX A
RESULTS OF ACTIVATION DYNAMICS OF EMG ENVELOPES

Tibialis Anterior, Gastrocnemius Lateralis, Gastrocnemius Medialis, Peroneus Longus

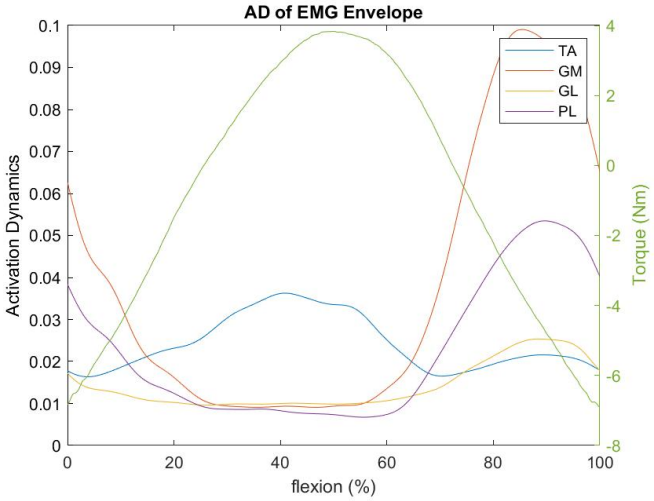

SUBJECT 1

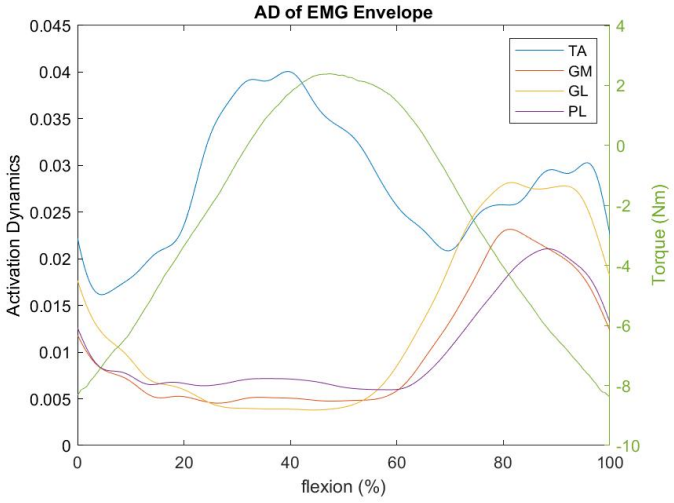

SUBJECT 2

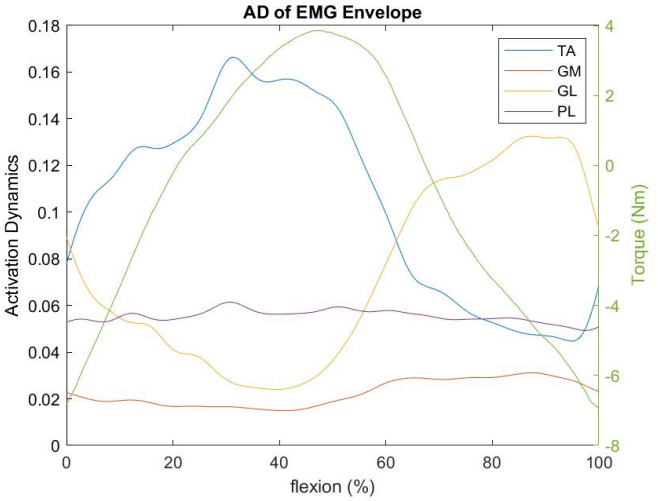

SUBJECT 3

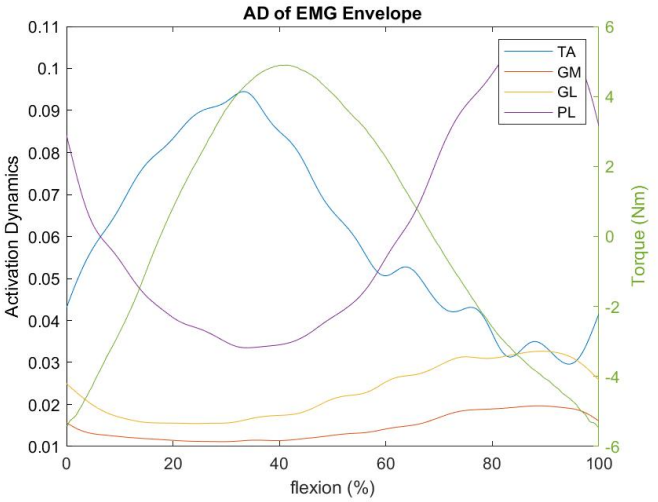

SUBJECT 4

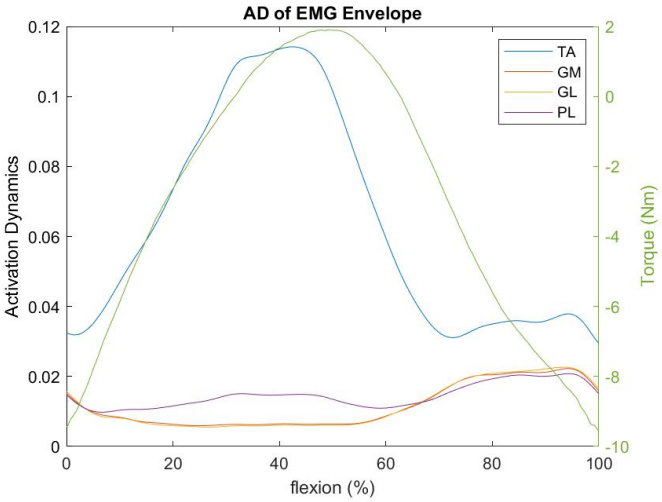

SUBJECT 5

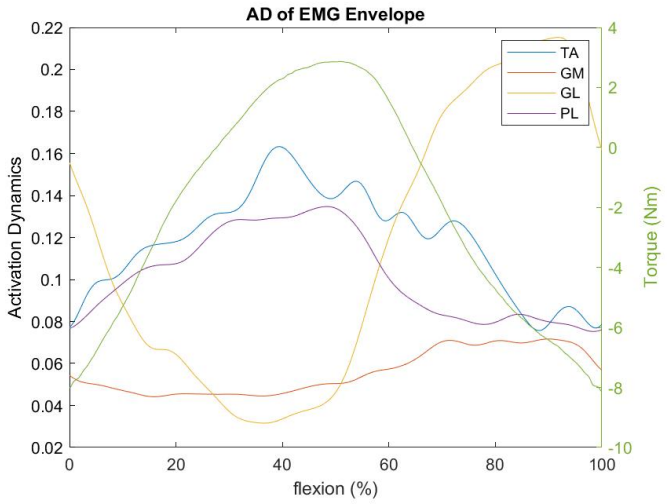

SUBJECT 6

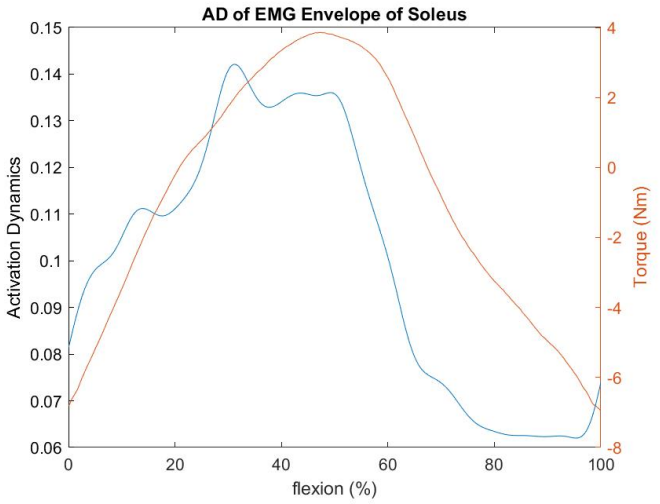

SUBJECT 3

Soleus

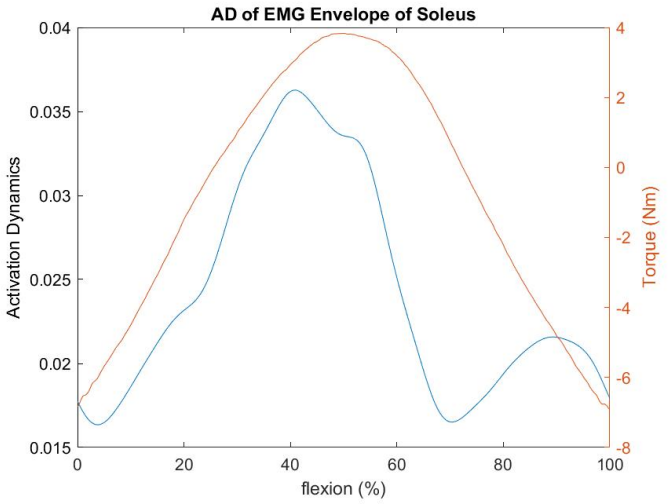

SUBJECT 1

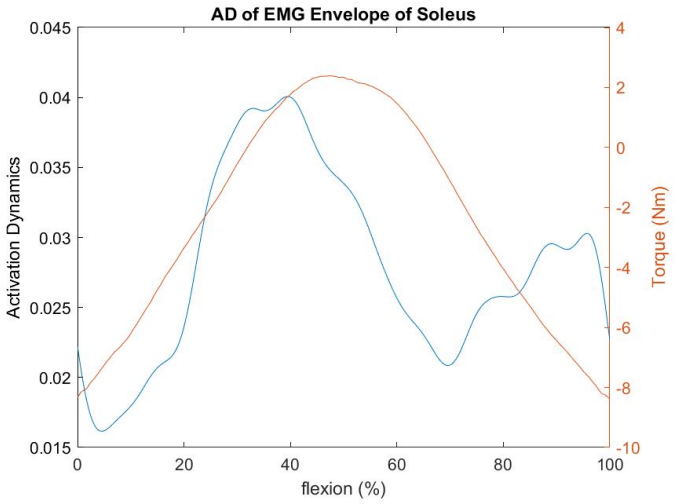

SUBJECT 2

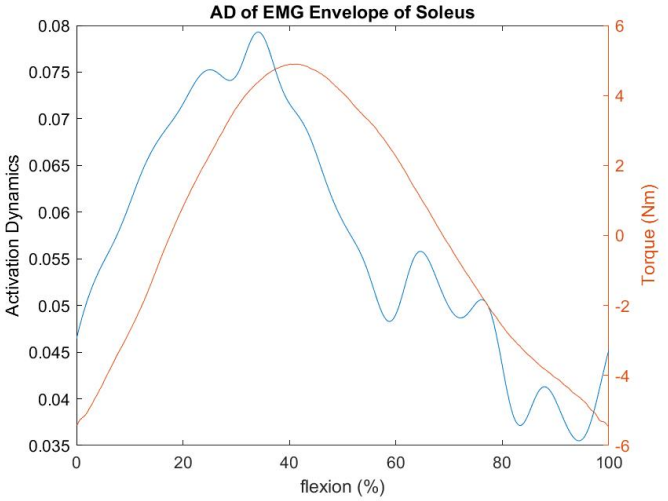

SUBJECT 4

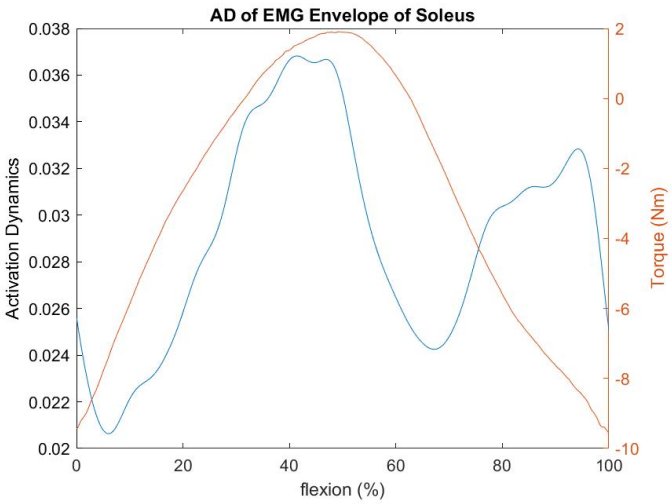

SUBJECT 5

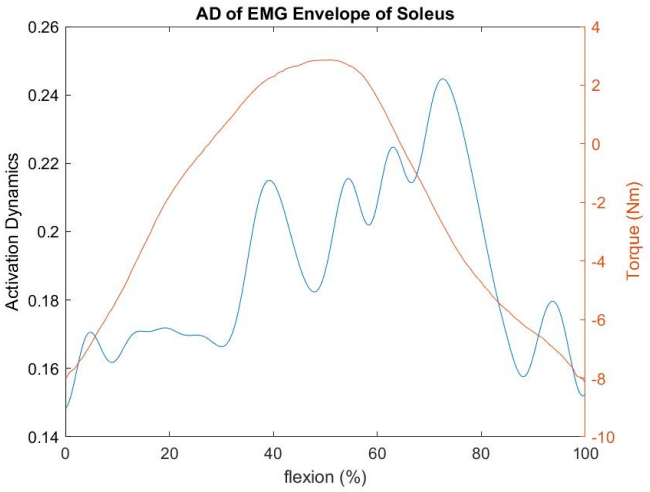

SUBJECT 6

APPENDIX B

RESULTS OF ACTIVATION DYNAMICS OF MOTOR UNITS

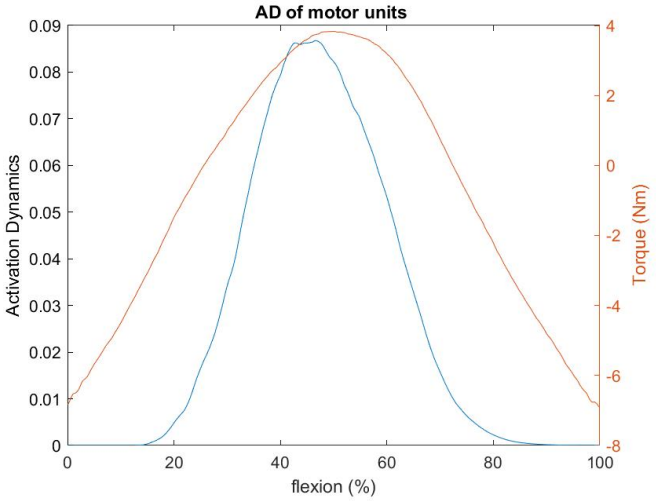

SUBJECT 1

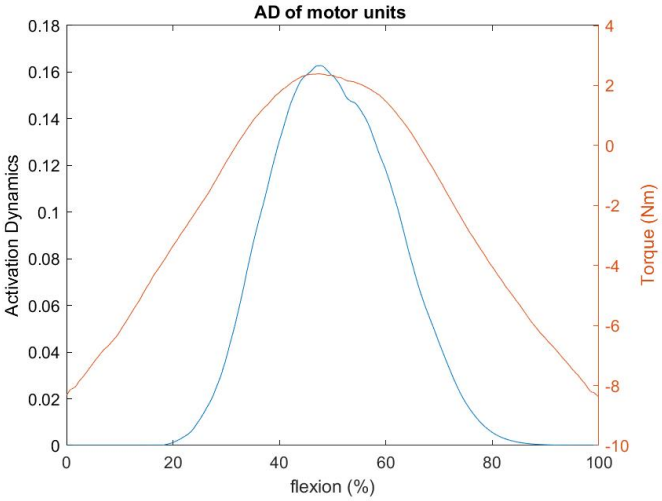

SUBJECT 2

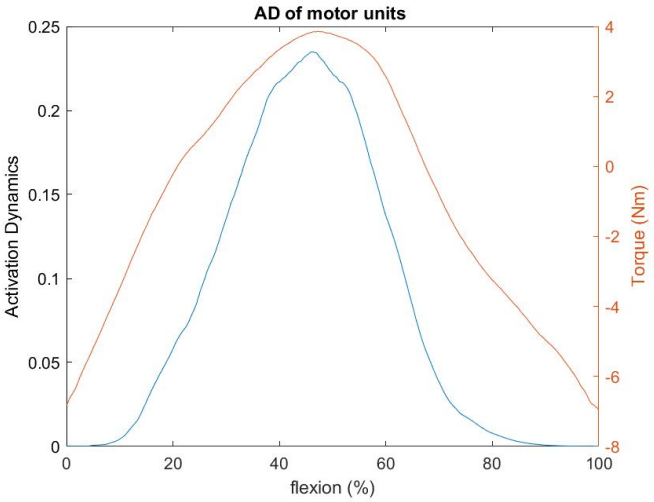

SUBJECT 3

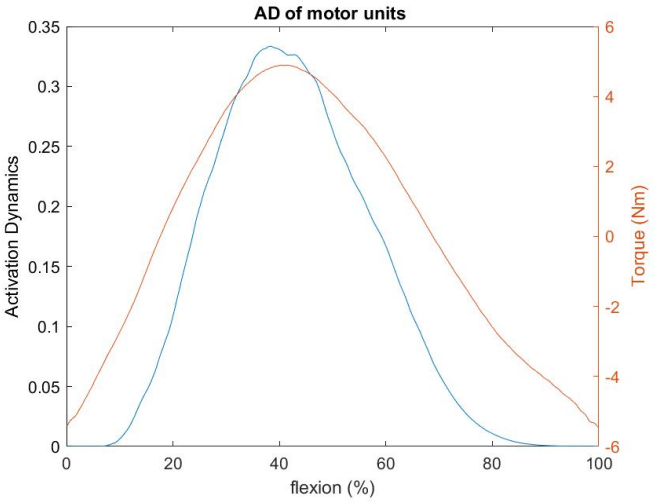

SUBJECT 4

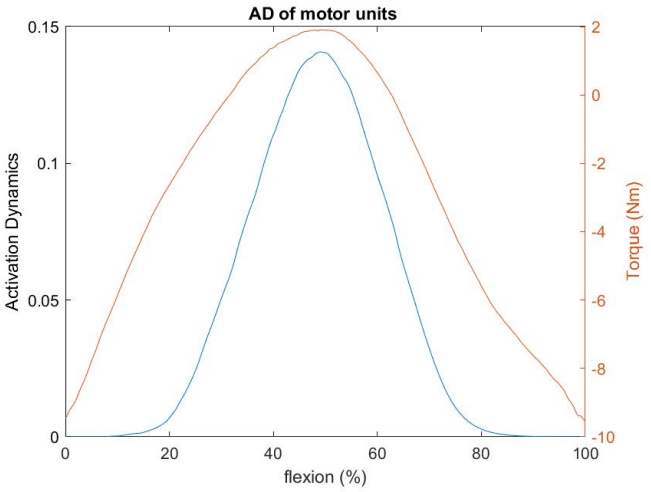

SUBJECT 5

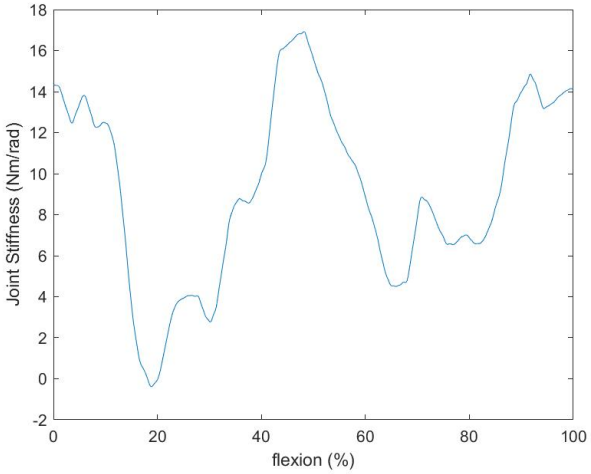

SUBJECT 1

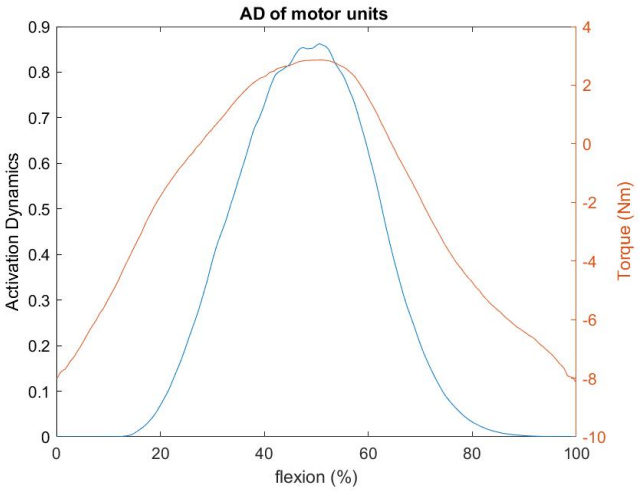

SUBJECT 6

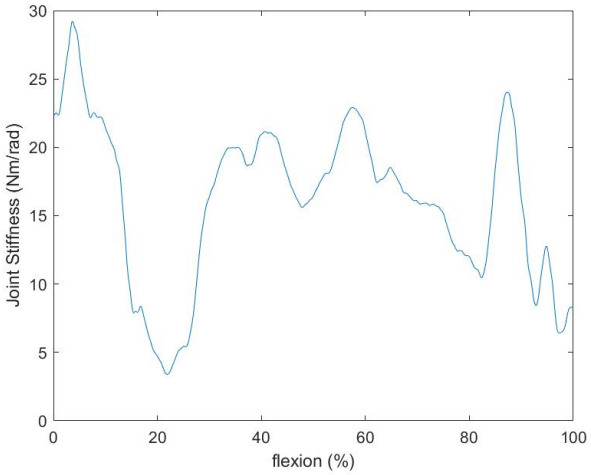

SUBJECT 2

APPENDIX C

INDIVIDUAL STIFFNESS THROUGH SYSTEM IDENTIFICATION

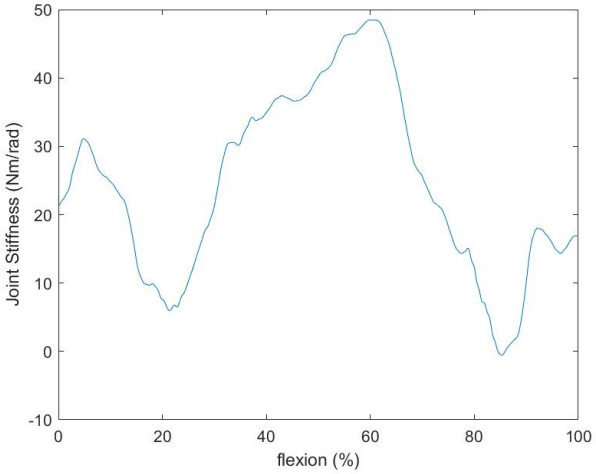

SUBJECT 3

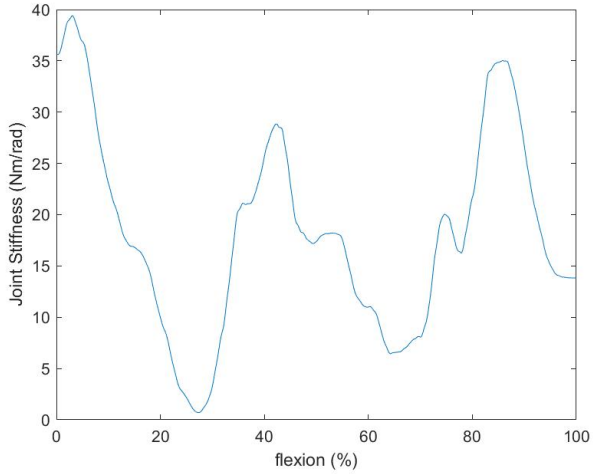

SUBJECT 4

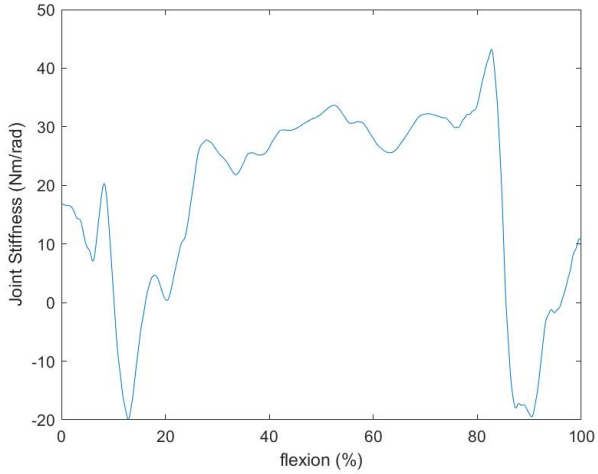

SUBJECT 5

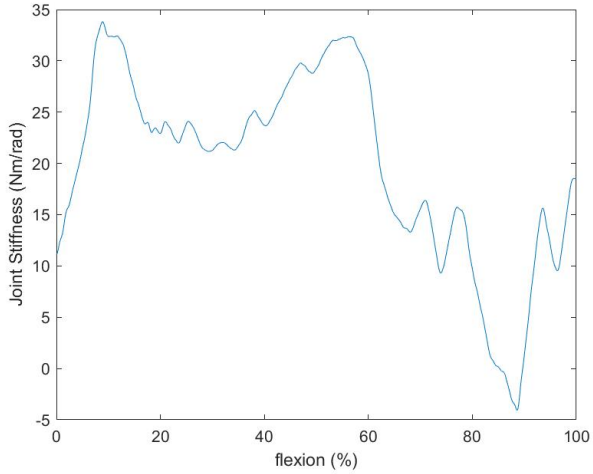

SUBJECT 6

APPENDIX D
COMPARISON RESULTS: PREDICTED TORQUES AND REFERENCE TORQUE

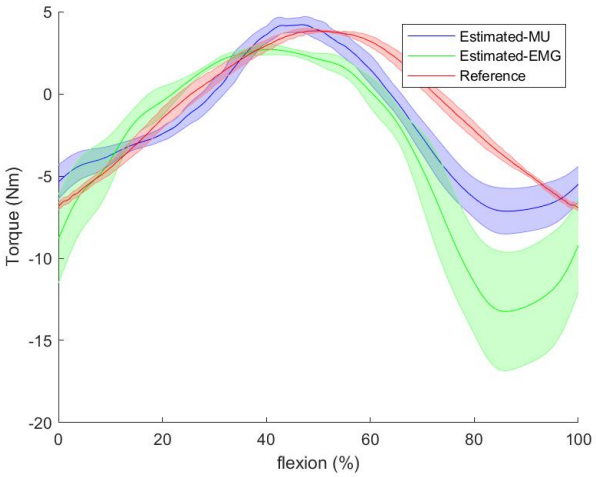

SUBJECT 1

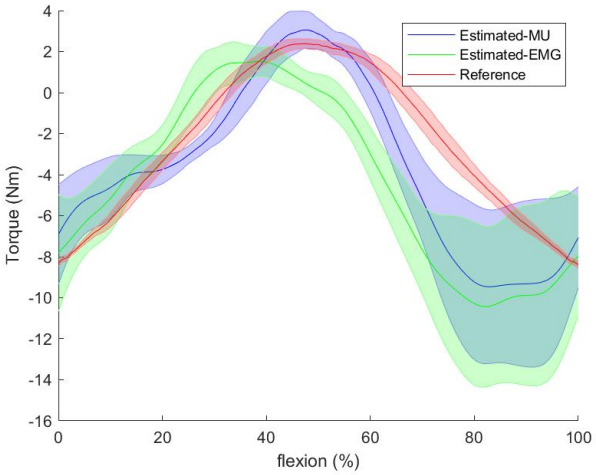

SUBJECT 2

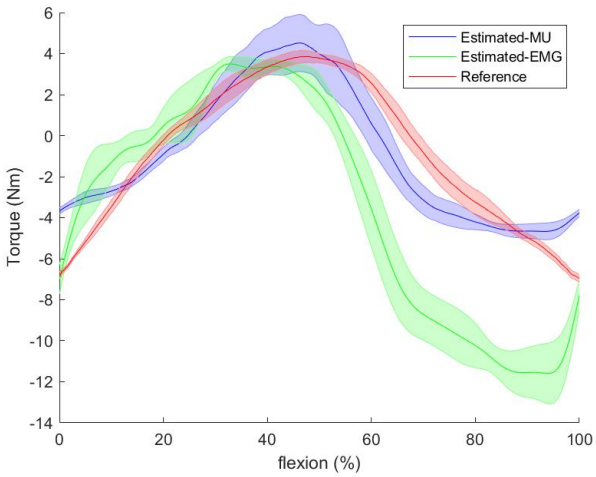

SUBJECT 3

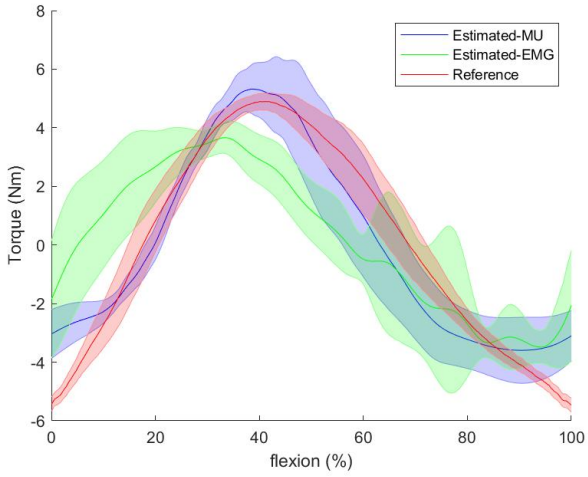

SUBJECT 4

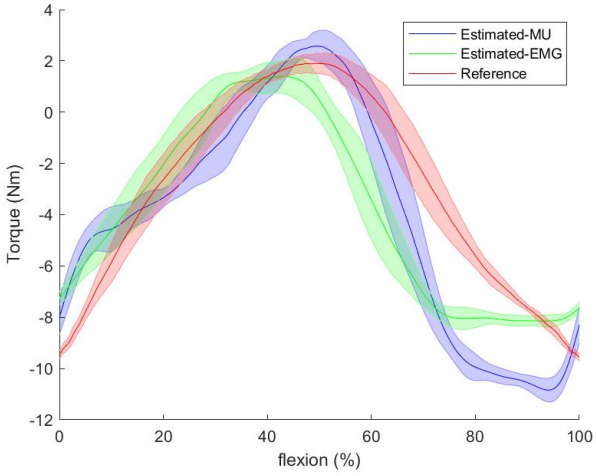

SUBJECT 5

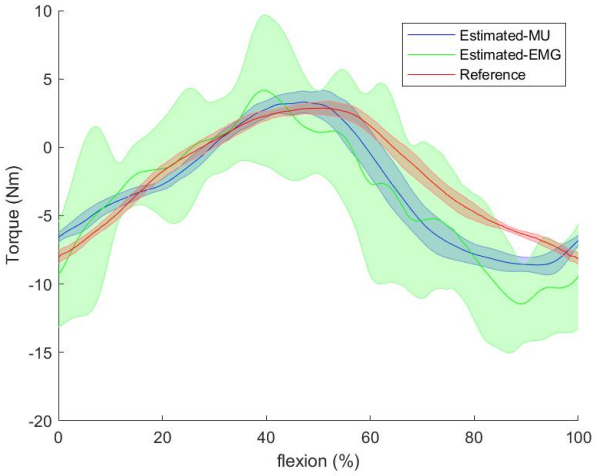

SUBJECT 6

APPENDIX E
COMPARISON RESULTS: PREDICTED STIFFNESS AND REFERENCE STIFFNESS

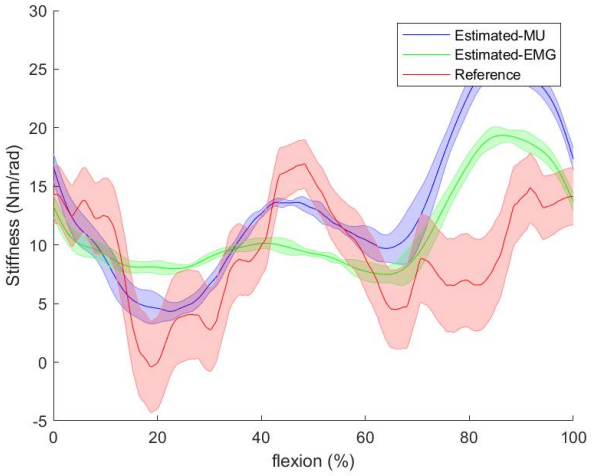

SUBJECT 1

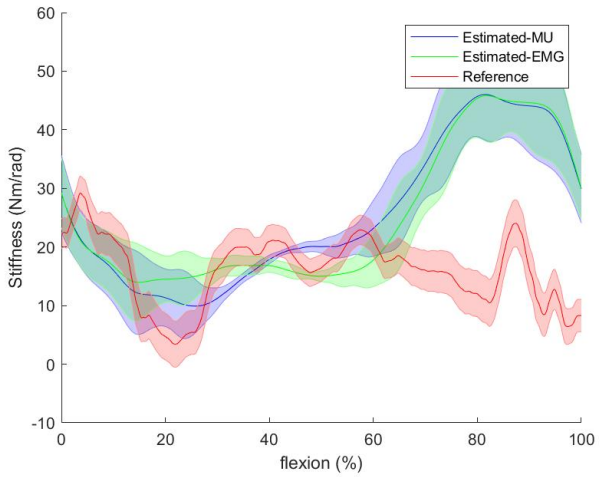

SUBJECT 2

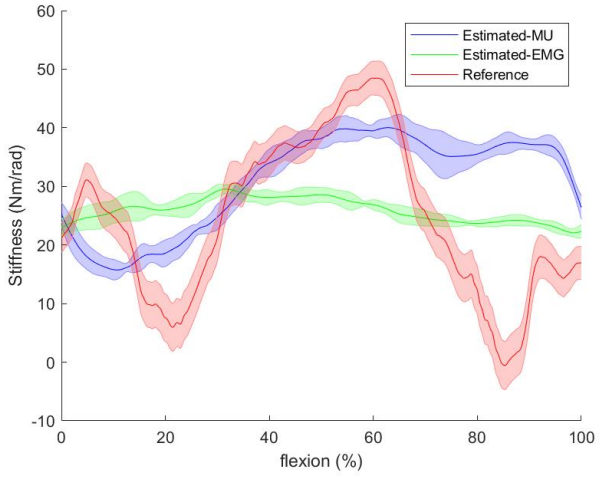

SUBJECT 3

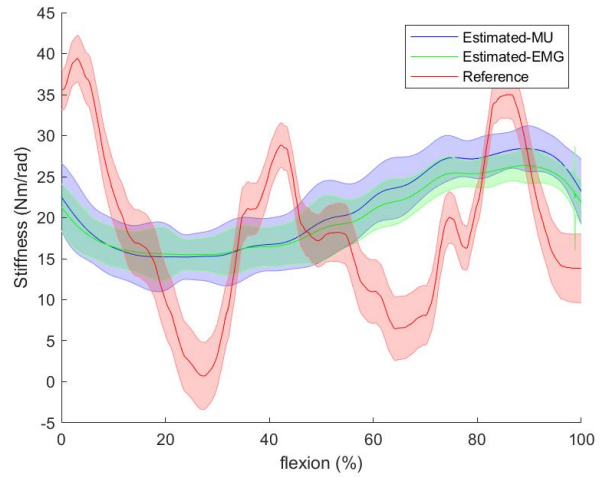

SUBJECT 4

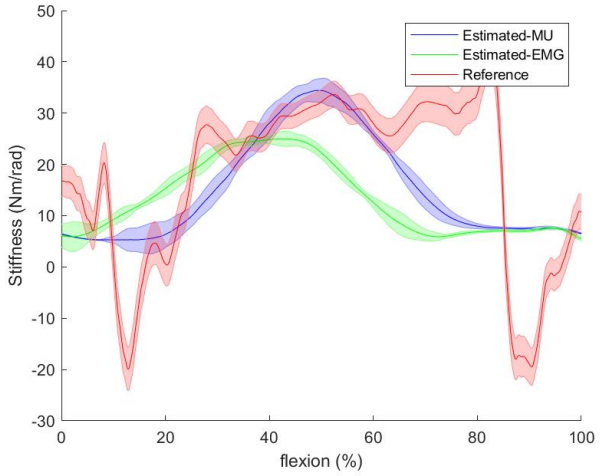

SUBJECT 5

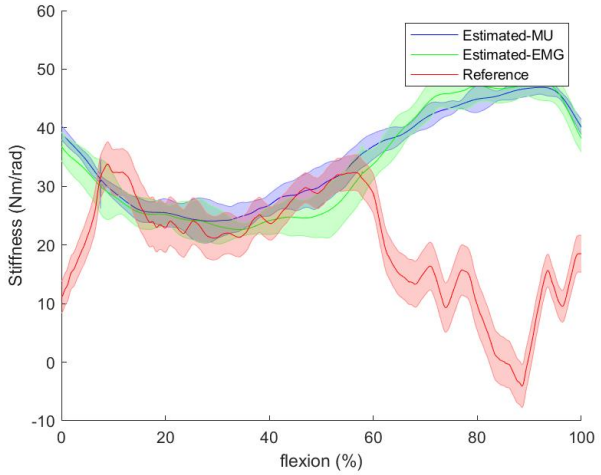

SUBJECT 6

APPENDIX F

NUMERICAL RESULTS: COMPARISON OF EXPERIMENTAL TORQUE AND STIFFNESS ESTIMATIONS VIA SYSTEM IDENTIFICATION AGAINST ESTIMATED TORQUE AND ESTIMATED STIFFNESS VIA MODEL DRIVEN USING AD OF EMG ENVELOPES AND AD OF MOTOR UNITS

MEAN OF ALL SUBJECTS

		RMSE (Nm)/(Nm rad^{-1})	nRMSE	R^2	Min. Stiff (Nm rad^{-1})	Max. Stiff (Nm rad^{-1})
Torque	AD of EMG Envelope	5.98	1.38	0.42	-	-
	AD of motor units	2.70	0.62	0.70	-	-
Stiffness	AD of EMG Envelope	15.53	0.78	0.13	8.51	37.16
	AD of motor units	16.34	0.83	0.17	7.57	39.57
	System Identification	-	-	-	-3.46	35.09

SUBJECT 1

		RMSE (Nm)/(Nm rad^{-1})	nRMSE	R^2	Min. Stiff (Nm rad^{-1})	Max. Stiff (Nm rad^{-1})
Torque	AD of EMG Envelope	5.05	1.33	0.54	-	-
	AD of motor units	2.42	0.63	0.74	-	-
Stiffness	AD of EMG Envelope	6.16	0.60	0.09	4.99	29.85
	AD of motor units	8.58	0.84	0.19	1.92	28.37
	System Identification	-	-	-	-0.393	16.92

SUBJECT 2

		RMSE (Nm)/(Nm rad^{-1})	nRMSE	R^2	Min. Stiff (Nm rad^{-1})	Max. Stiff (Nm rad^{-1})
Torque	AD of EMG Envelope	4.69	1.03	0.4	-	-
	AD of motor units	3.56	0.77	0.6	-	-
Stiffness	AD of EMG Envelope	19.36	1.14	0.04	5.62	28.69
	AD of motor units	19.14	1.12	0.03	6.56	27.23
	System Identification	-	-	-	3.39	29.2

SUBJECT 3

		RMSE (Nm)/(Nm rad^{-1})	nRMSE	R^2	Min. Stiff (Nm rad^{-1})	Max. Stiff (Nm rad^{-1})
Torque	AD of EMG Envelope	6.135	1.50	0.397	-	-
	AD of motor units	2.46	0.60	0.675	-	-
Stiffness	AD of EMG Envelope	13.66	0.49	0.10	16	40
	AD of motor units	18.41	0.66	0.11	5	63
	System Identification	-	-	-	-0.5	48

SUBJECT 4

		RMSE (Nm)/(Nm rad^{-1})	nRMSE	R^2	Min. Stiff (Nm rad^{-1})	Max. Stiff (Nm rad^{-1})
Torque	AD of EMG Envelope	3.39	0.86	0.43	-	-
	AD of motor units	1.85	0.47	0.82	-	-
Stiffness	AD of EMG Envelope	12.04	0.58	0.08	10.27	26.4
	AD of motor units	13.31	0.64	0.08	9.68	26.98
	System Identification	-	-	-	0.71	39.41

SUBJECT 5

		RMSE (Nm)/(Nm rad^{-1})	nRMSE	R^2	Min. Stiff (Nm rad^{-1})	Max. Stiff (Nm rad^{-1})
Torque	AD of EMG Envelope	2.94	0.58	0.60	-	-
	AD of motor units	3.11	0.60	0.683	-	-
Stiffness	AD of EMG Envelope	17.21	0.71	0.10	2.01	29.44
	AD of motor units	15.52	0.64	0.23	4.49	38.45
	System Identification	-	-	-	-19.9	43.21

SUBJECT 6

		RMSE (Nm)/(Nm rad^{-1})	nRMSE	R^2	Min. Stiff (Nm rad^{-1})	Max. Stiff (Nm rad^{-1})
Torque	AD of EMG Envelope	13.66	2.97	0.13	-	-
	AD of motor units	2.82	0.61	0.70	-	-
Stiffness	AD of EMG Envelope	24.72	1.13	0.35	12.19	68.56
	AD of motor units	23.06	1.05	0.36	17.75	53.41
	System Identification	-	-	-	-4.08	33.82

APPENDIX G
SUMMARY OF THE ENTIRE STUDY

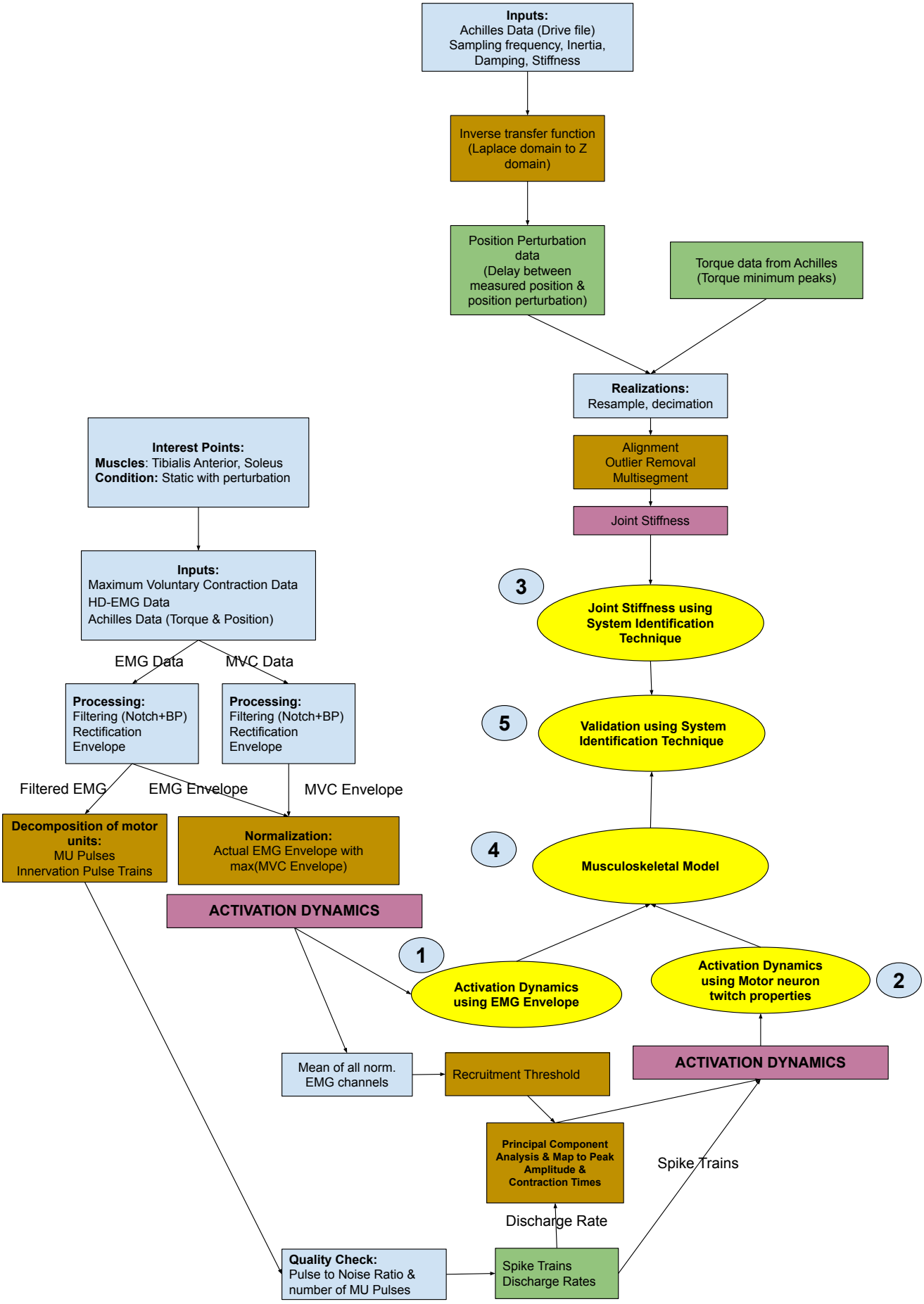

Fig. 27: Schematic diagram of the musculoskeletal model that combines stiffness estimation and the identification of motoneuron properties. 1 to 5 are the major processes while the rest are the steps involved in the processes.